NASA Technical Memorandum 84358

Flight Test Results of the Strapdown Ring Laser Gyro Tetrad Inertial Navigation System

R. A. Carestia, R. J. Hruby and W. S. Bjorkman

October 1983

NASA
National Aeronautics and
Space Administration

NASA Technical Memorandum 84358

Flight Test Results of the Strapdown Ring Laser Gyro Tetrad Inertial Navigation System

R. A. Carestia, University of Southern Colorado, Pueblo, Colorado
R. J. Hruby, Ames Research Center, Moffett Field, California
W. S. Bjorkman, Analytical Mechanics Associates, Mountain View, California

NASA
National Aeronautics and Space Administration

Ames Research Center
Moffett Field, California 94035

SUMMARY

A helicopter flight-test program undertaken to evaluate the performance of Tetrad — a strap-down, laser-gyro, inertial navigation system — is described. The results of 34 flights show a mean final navigational velocity error of 5.06 knots, with a standard deviation of 3.84 knots; a corresponding mean final position error of 2.66 n. mi., with a standard deviation of 1.48 n. mi.; and a modeled mean-position-error growth rate for the 34 tests of 1.96 knots, with a standard deviation of 1.09 knots. No laser-gyro or accelerometer failures were detected during the flight tests. Off-line parity-residual studies used simulated failures with the prerecorded flight test and laboratory test data. The airborne Tetrad system's failure-detection logic, exercised during the tests, successfully demonstrated the detection of simulated "hard" failures and the system's ability to continue successfully to navigate by removing the simulated faulted sensor from the computations. Tetrad's four-ring laser gyros provided reliable and accurate angular-rate sensing during the 4 yr of the test program, and no sensor failures were detected during the evaluation of free-inertial navigation performance. The original scale factor and cross-coupling parameter calibration made in the laboratory during initial assembly was never significantly improved upon. Repeated checks of the laser-gyro bias compensation showed it to be stable for the duration of the evaluation.

INTRODUCTION

The Tetrad inertial navigation system is an experimental, strap-down system which features laser gyros as rotation sensors. Laser gyros, illustrated in figure 1, were little known at the time (1977) the Tetrad was developed. They are now widely accepted as rotation sensors for inertial reference systems (IRS) because of their simplicity, reliability, and calibration stability. The Tetrad's developer, Honeywell, Inc., had demonstrated the feasibility of using laser gyros in strap-down inertial navigators through tests of the Honeywell LINS system in fixed-wing aircraft prior to production of the Tetrad system. However, nothing had been demonstrated, except at Honeywell, about the long-term bias stability of the laser gyro or its reliability in avionics systems. The possibility of utilizing a strap-down inertial system in helicopters had never been demonstrated. In the time since creation of the Tetrad, laser gyros have come to rival wheel gyros for many sensing applications (e.g., the IRS in Boeing's 767).

The Tetrad system contains a unique redundancy feature for studying system reliability in the presence of the inertial sensor failures. The Tetrad includes one extra gyro and one extra accelerometer, both mounted in a skewed configuration so they can be used to detect and isolate failures in any of the other three sensors. This is shown in figure 2, which illustrates the inertial sensor assembly (ISA). This redundant configuration was developed to enable reliability studies with a four-axis IRS for aircraft (see refs. 1-7). The Tetrad was the second redundant inertial navigation system evaluated at Ames Research Center. An earlier evaluation effort (ref. 8) involved a hexad (six-axis) inertial reference unit, Draper Laboratories'

strap-down inertial reference unit (SIRU). The SIRU inertial navigation system utilized conventional wheel gyros and was flown in a fixed-wing aircraft (CV-340).

The three primary objectives of the Tetrad test program reported here were (1) to determine the effects of helicopter flight environment on a strap-down inertial reference and navigation system; (2) to assess the capability of a Tetrad (four-axis) inertial reference unit for detecting and isolating sensor failures with the intent of improving system reliability; and (3) to establish a baseline for the long-term calibration stability of laser gyros and resultant operational characteristics of IRSs based on such gyros. Supporting documentation for the system description and for the related project (SIRU Flight Test Program) are contained in references 8-10.

The remainder of this paper is organized into four sections, the first of which contains a system description of the Tetrad, a brief introduction to laser gyros, and a short presentation of the use of the parity-residual as a failure-detection/isolation criterion. The test procedures and objectives are then defined and the test program results are presented. The final section presents the conclusions derived from the program. Appendixes A through D contain supporting details on test data recording and evaluating software; the parity-residual sensor-failure-detection algorithm; Tetrad system software; and the Three-Axis Motion Simulator Facility.

TETRAD SYSTEM DESCRIPTION

System Overview

The Tetrad is a free-inertial navigation system which utilizes a strap-down-configuration laser-gyro inertial sensor array (ISA); the ISA is shown in figure 2. The sensor array consists of four single-degree-of-freedom laser gyros and four linear accelerometers. Three sensing axes of the ISA lie along the orthogonal axes of a cube and the fourth sensing axis (skew axis) lies along the cube's diagonal, as illustrated in figure 3. Each axis contains one laser-rate gyro module and one linear accelerometer module which senses linear acceleration along the input axis. The purpose of the fourth laser gyro and accelerometer is to enable fault detection and to study redundancy management algorithm performance.

The Tetrad inertial navigation system (INS) uses two Honeywell H301 (ruggedized) airborne computers. All of the navigation software, as well as the sensor compensation, attitude computation, failure-detection, redundancy management, and panel control logic, is contained in the system navigation computer (SNC). The auxiliary computer (called CPU No. 2) receives data from the SNC and, after conditioning the data, sends it out to (1) a nine-track digital magnetic tape, (2) digital-to-analog ports, or (3) a serial digital transmitter. A time-code generator and a cycling DME receiver feed time and range data into CPU No. 2 to provide external references to be recorded with Tetrad data for postflight evaluation (see appendix A) of system performance. The Tetrad Flight System components are illustrated in figure 4, and the flight hardware system with its ground support is shown in figure 5. The test aircrafts were a UH-1H helicopter (fig. 6) and a UH-1B helicopter.

Laser-Gyro Features

The laser gyro is a relatively new device which offers — in comparison with electromechanical gyros of comparable performance — the potential of increased reliability, simpler operational characteristics, and lower cost. A typical laser gyro is illustrated in figure 1. When the gyro is rotated about its sensing axis, a phase shift results which is a measure of the rate of rotation of the gyro in inertial space. One count corresponding to 1.6 arc seconds is produced for each multiple of 180° of optical phase shift.

A principal advantage of the laser gyro from an operational point of view is its long-term bias stability. Compensation values remain constant to within about 0.01°/hr over a period of years, so the system need not be frequently recalibrated. Another significant advantage of laser gyros over wheel gyros is that the laser gyro requires no compensation for acceleration-induced drifts, such as mass unbalance or anisoelastic drifts.

Failure Detection by Parity-Residual Monitoring

The skewed, redundant, laser-gyro sensor configuration, combined with faulted-sensor detection and identification software, would permit the inertial sensing system to function when any three gyros (out of four) and any three accelerometers are operational. When a sensor failure is detected and identified, it can be excluded by system software from the computations of position, velocity, and attitude, thereby allowing the system to continue to function with the remaining three sensors. Without auxiliary means of failure identification, the Tetrad can only detect a failure. It cannot identify the faulted sensor. Methods of identifying the faulted sensor are discussed in references 3-7. Failure tests of the Tetrad system were concerned only with detection capability.

The Tetrad's failure-detection algorithm utilizes the "parity-residual" as an indication of sensor failure. In the ortho-skew configuration, the output of any one sensor can be formulated as a linear combination of the outputs of the other three sensors. The difference between a sensor's output and its formulated output based on the other sensors is called the parity-residual. Since normal instrument errors and output quantization cause this relationship to be imperfect, the parity-residual takes on a small range of nonzero values during normal operation. This is illustrated in figure 7, which shows parity-residual amplitude versus time. A persistent sensor fault can be detected by summing the parity-residual over a specified moving window time-interval; this is illustrated in figure 8. The parity-residual was generated each 0.025 sec (the navigation update rate) in the Tetrad mechanization. "Noise" in the parity-residual is primarily created by the Tetrad's 1.57-arc-second gyro resolution. Only the parity-residual detection algorithm was evaluated. Appendix B explains the theory of failure detection by observation of the parity-residual. Earlier research results have shown that the parity-residual failure algorithm had the capability to detect wheel-type attitude, step-type gyro drift failures as small as 0.03°/hr (refs. 3, 8).

TEST PROCEDURES

The purpose of the Tetrad test program was to evaluate laser-gyro, strap-down inertial techniques for use in integrated guidance and control systems for VTOL

aircraft. This was to be achieved by flight testing the Tetrad system in helicopters and by laboratory investigations to evaluate its performance. Appendix A describes the data reduction and performance evaluation. Similar methods are reported in reference 8.

The flight- and laboratory-test programs included both short (1-hr) and long (3-hr) test periods, straight and triangular flight segments, curved paths, and conventional terminal-area maneuvers. This section describes the test program, including

1. Operational procedures used to prepare and operate the Tetrad system

2. Tetrad flight-test procedures

3. A description of the VTOL aircraft position reference system

4. Use of data analysis algorithms to reduce and analyze the test data, using Ames Research Center's IBM-360 or CDC-7600 computers

5. Laboratory motion simulator used in the test program

6. Sensor-failure detection test procedure

Figure 9 is a block diagram of the Tetrad computer system. It includes dual computers, digital tape recorder, control interface box, and the computer display unit (CDU). For programming and internal computer control, a system software evaluation unit (SSEU) was utilized; it is also shown.

The Tetrad's two computers were mechanized to run in basic and research modes, respectively. The basic computer transmitted selected output data, such as attitude, position, velocity, and status data, to the research computer for additional conditioning. The research computer received data from the basic computer through an interrupt and register-to-register transfer. The Tetrad software system is described in appendix C.

Tetrad Operational Procedures

To accomplish the objectives of the test program, the flight-testing procedures were designed to reflect standard user operating procedures as closely as possible. Hence, a typical flight test required less than 20 min of preflight activity to initialize the Tetrad system for use and generally 10 min or less for alignment. A typical preflight test procedure is as follows:

1. Tetrad power switched to standby for a period of 0.5-2 hr (depending on the flight objective) to bring the Tetrad to operational temperature. This was done on ground power and is consistent with current preflight procedures.

2. Once aircraft power had been established, the Tetrad flight system was turned to standby again for up to 10 min or long enough to remove temperature transients.

3. The internal alignment was performed on aircraft power during a 3-10-min period, after which Tetrad was switched to the navigation mode. Midway through the

test program, software was incorporated to have the switching from alignment to navigation done automatically following a preset 5-min alignment interval.

Flight-Test Procedures

The flight-test program consisted of 34 flights, all of which began and ended at Moffett Field, California. The landmarks used at Moffett Field are shown in figure 10. Crows Landing Naval Auxiliary Landing Field facilities (Crows Landing, Calif.) were utilized for eight of the 34 flight tests. All flights were made in California's San Joaquin and Santa Clara valleys. The most commonly flown path was from Moffett Field to the Calavaras, San Antonio, and Del Valle reservoirs following a roughly triangular ground track. Figure 11 shows the flight-test area and the landmarks used as visual navigation references. Figure 12 shows the distance-measuring equipment (DME) stations used for radio range reference. The flight-test program was devoted to free-inertial navigation performance, but early flights were used additionally for calibration verification and system adjustments. The test flights made near Crows Landing provided performance data during turns, takeoff, and landing maneuvers, using ground-based radar as a position reference. All flights were conducted at altitudes below 1524 m (5000 ft). The Crows Landing test facility and the landmarks used in the eight test flights are shown in figure 13.

Flight-test patterns were of two types: en route (from Moffett Field to Crows Landing or the reservoirs and return) and triangular (flights between the three above-mentioned reservoirs, landmarks 3, 4, and 5 of fig. 11). The en route pattern consisted of a departure from Moffett Field, a turn to fly over the Moffett DME, cruise to the test area (reservoirs), execution of a triangular test pattern, and then return to Moffett. The triangular pattern consisted of cruising between the reservoirs, and executing 360° turns at each reservoir. The same route sequence, in reverse order, was used on returning to Moffett Field (the flyover of the DME was optional).

VTOL Aircraft Position-Reference System

The continuous position-reference system used during the Tetrad flight tests to track the UH-1H aircraft consisted of two primary references: (1) a modified Nike-Hercules radar tracking system located at Crows Landing; and (2) a six-channel, multiple-DME-receiver system, designed by Sierra Research Cooperation, mounted within the aircraft.

The modified Nike-Hercules radar provided improved resolution through the use of "19-bit" range and angle digital shaft encoders, with atmospheric refraction correction provided. A transponder aboard the UH-1H was used to improve radar angle tracking.

The DME receiver system provided range information from up to six DME or TACAN stations. The system utilized a fast-switching DME receiver which was programmed to automatically switch through each of six preselectable DME or TACAN frequencies. Range lockup time was 1 sec maximum, and range output resolution was 18.5 m (0.01 n. mi.). Output range information was tagged with station frequency and receiver-clock time for identification.

Reference landmarks were also used throughout each flight to provide a third but intermittent position reference. The helicopters circled each landmark so that it

would be identified on the taped data by observing the recorded heading change if the DME data recording failed. The landmarks are shown in figure 11. The time at which each landmark was reached was also manually recorded by the copilot in order to correlate with radar or DME position data. During early flights in the UH-1B, an observer manually triggered a tape-mark as the craft hovered over the landmark to record the acquisition of a known reference position.

The chart in figure 12 shows the relative positions of the DME stations, radar system, and reference airports used during the flight tests. A list of the DME stations, their frequencies, and their locations is given in table 1. The range and bearing of each station are given with respect to the TACAN coordinates at Crows Landing. The acquisition altitude is the minimum altitude required at Crows Landing in order to receive a signal from the DME station (assuming line-of-sight transmission).

United States Geological Survey reference position landmarks and azimuthal lines at Moffett Field and Crows Landing were used to provide accurate start and terminal-area position fixes. The landmarks were located to within ±4.0 arc seconds of position (standard deviation). Table 2 lists the latitude, longitude, and elevation of the applicable landmarks surveyed for Moffett Field and Crows Landing, respectively. Figure 10 shows the location of the landmarks with respect to reference buildings and other features at Moffett Field, and figure 13 shows the landmarks at Crows Landing.

Data Analysis

Because of the limited aircraft utilization time available for the Tetrad flight test, a concerted effort was made to record a large amount of data during each test flight. All data necessary to reconstruct the flight history (positions, velocity, attitude, reference data, time codes, etc.) were recorded. Additionally, a 20-min period of raw sensor data was recorded on most flights. The Tetrad data are recorded digitally and the resultant magnetic tapes require no preprocessing or reformatting to be read on the H316, CDC 7600, or IBM 360 computers. The Tetrad's recording system is limited by its recording speed and by the total data storage capacity of the 8-in. magnetic tape reel. Appendix A describes the extensive library of data reduction and analysis computer programs used in processing Tetrad test data (ref. 1).

Motion Simulator Facility

The Motion Simulator Facility was developed at Ames Research Center for testing inertial-sensor-system concepts applicable to strap-down inertial sensors. This facility was used to augment the flight-test program by providing a convenient, controlled, nonstationary operating environment for the Tetrad INS. The facility included a three-axis gimbaled table, two minicomputers, a dual, floppy-disk-based microcomputer, two digital magnetic tape recorders, a line printer, and other peripherals required for detailed system testing. An adapter plate was built to allow the laser-gyro Tetrad inertial sensor assembly (ISA) to be installed on the motion simulator. The minicomputer system is shown in figure 14, the motion simulator with the laser-gyro ISA is shown in figure 15, and the block diagram of its data acquisition system is shown in figure 16. A description of this test facility is presented in appendix D.

Sensor-Failure Detection-Test Procedure

The failure-detection algorithm was tested off-line, using prerecorded experimental data and simulated sensor failure. These data samples were generated on a three-axis (see appendix D) motion simulator and, during the flight test of the Tetrad INS, in the UH-1H research aircraft. Data were recorded at approximately 40 Hz. The failures were introduced off-line in a simulated rerun of a small time-segment of the real-time experiment, using the CDC 7600 Ames computer facility. This allowed a systematic variation of test variables under repeatable test conditions.

FLIGHT AND LABORATORY TEST RESULTS

The Tetrad inertial navigation system was accepted from Honeywell in January 1977; it was then prepared for flight and laboratory testing that began in February 1977 and continued through June 1980. Static acceptance tests were conducted from April 1977 through May 1977 in preparation for flight tests. From June 1977 through November 1977 Tetrad was exercised in the free-inertial mode in a UH-1B helicopter. Its accuracy was checked, using optically sighted position reference markers, during each flight test in the vicinity of Moffett Field (benchmarks A, B, and D, fig. 10). The Tetrad was the only flight experiment installed in the UH-1B during this period. Although equipment malfunctions occurred intermittently throughout the 4-yr test period, Tetrad accuracy stayed within the original specifications. Malfunctions were usually found in cabling or power supplies and were never identified as sensor failures. Table 3 shows the flight-test data for 1977. There were 12 separate tests for a total of 17.86 navigation hours. In table 4, the tilt-drift "best estimate" error model was used to evaluate performance. The tilt-drift error model is the "best estimate" of the navigation position-error growth found by fitting a classical one-dimensional position-error model to the observed position errors using a least-squares-error fit. This approach provides a navigation best-estimate position-error growth value for each flight, as well as tilt angle and gyro-drift error estimates. The tilt-drift model is explained in appendix A. The final velocity error for the seven flight tests of 1977 was 3.8 knots, with a standard deviation of 2.93 knots in the triad (three-sensor) mode of operation. The corresponding mean final position error was 1.8 n. mi., with a standard deviation of 2.0 n. mi.

For the Tetrad (four-sensor) mode, the final velocity error for the seven flights was 3.6 knots, with a standard deviation of 2.8 knots. The corresponding mean final-position error was 1.38 n. mi., with a standard deviation of 1.12 n. mi. The average flight duration was 1.06 hr.

Flight-Test Results

During 1978, the flight-test system was modified to include a six-channel DME whose six near-simultaneous range words were referenced when the results were recorded (one or more per second). Six separate flight tests were made in November and December for a total of 5.8 hr of usable navigation. The results of the individual tests are shown in table 5, and the error and performance analysis results are given in table 6.

The mean final-position error for 1978 tests in the triad mode was 4.5 n. mi., with a standard deviation of 1.6 n. mi. The corresponding mean final-velocity error was 9.9 knots, with a standard deviation of 1.6 knots. The navigational portions of

these flights averaged about 80 min. The corresponding position and velocity errors for the Tetrad mode were 5.04 n. mi., with 0.77-n. mi. standard deviation, and 6.63 knots with a 1.8-knot standard deviation. The average flight duration was about 1.3 hr. The excessive size of the navigation error growth (9 knots) in the triad mode was not explained but may have been a result of electrical interference derived from the UH-1H power system and poorly executed alignments under adverse (gusty) wind conditions. The multiple-DME ranges provided satisfactory position data, and optical correlation with landmarks helped compensate for signal dropouts. The DME position data were correlated with optical sightings, using a 360° maneuver over each landmark.

The Tetrad was shifted from the UH-1H helicopter equipped with a digital flight control system (V/STOLAND) to another UH-1H in January 1979 to facilitate scheduling of experiments. During this reinstallation period, the laser gyros were remounted with new fasteners. It was found necessary to recalibrate the gyro biases after the remounting because screw torques were different and it affected the biases significantly. Following static laboratory measurements in May, 11 flight tests were conducted from late May through early June for a total of 10 hr of navigation. The 1979 flight data are presented in table 7, and the tilt-drift model best-estimate error analysis is shown in table 8. In the triad mode, the mean-position error was 2.2 n. mi., with a standard deviation of 1.1 n. mi. The triad mode mean-velocity error was 5.42 knots, with a standard deviation of 1.5 knots. In the Tetrad mode, the corresponding mean position error was 2.6 n. mi., with a standard deviation of 0.72 n. mi. The Tetrad mode mean-velocity error was 5.7 knots, with a standard deviation of 1.8 knots. The Tetrad mode showed slightly less accuracy than the triad mode in spite (or perhaps because) of the redundant sensing axis. The average flight duration was 0.85 hr. The analysis of the 1979 results led to a recalibration attempt of the scale factors and misalignments by Honeywell in the fall of 1979. The expected improvement in navigation accuracy did not materialize for the Tetrad mode because the nominally vertical accelerometer was not functioning properly and could not be calibrated, demonstrating an erratic bias. The calibration misalignment and scale factor of the skewed sensor of either type was less determinate than the calibration for the orthogonal sensor because of calibration procedural difficulties. The three "good" sensor sets (laser gyro and accelerometers) were installed in the orthogonal axes and laboratory calibration tests were then completed (see ref. 10).

Following several months of additional laboratory motion and nonmotion (static) tests conducted to establish the operability and the basic navigational accuracy of the Tetrad system, seven flight tests were conducted in the triad mode and two additional tests were conducted in the Tetrad mode for diagnostic purposes, for a total of 11.5 hr. Each flight test was preceded by a 5-min alignment.

Because the skewed-axis accelerometer exhibited erratic output (which could not be calibrated) it was not used. The tests showed a triad-mode mean final-position error of 3.13 n. mi. with a standard deviation of 1.1 n. mi. and a mean final-velocity error of 5.4 knots with a standard deviation of 2.6 knots. The average flight duration was 1.62 hr. Table 9 shows the reduced flight data and table 10 shows the results of the postflight tilt-drift best-estimate error analysis. The test sequence in 1980 showed a slight loss of accuracy, perhaps a result of equipment problems. There was not a strong correlation between alignment time and the navigation errors in position and velocity when alignment duration was longer than about 2 min. This is illustrated in figure 17 in which the final-velocity error and the tilt-drift best-estimate velocity error are plotted versus alignment time for all usable flight-test segments from all 4 yr for which the minimum alignment time was 2 min or more.

The Tetrad's performance remained stable during the 4-yr period. This fact is illustrated in tables 11 and 12, which show the mean and standard deviations for each test group for position and velocity.

The navigational errors are summarized against time into the test program in figures 18 and 19. The first of these shows velocity error; the second shows position error. Both final and modeled errors are presented. The final errors are not normalized with respect to navigation duration and would generally be larger for longer tests.

Laboratory Test Results

The initial static navigation acceptance tests were conducted in April 1977. Position error in nautical miles is shown as a function of time in figure 20 for this test. A straight-line fit to the final position error indicates an error growth rate of about 1.1 knots; however, termination of the test at some other time could have resulted in either a larger or smaller error growth-rate value and illustrates the need for an error model that will provide more insight to the error sources. The tilt-drift error model described in appendix A was used to normalize experimental data such as that shown in figure 21 — alignment errors (tilts) or gyro drifts.

In December 1977 a series of static laboratory tests was conducted to establish a baseline for evaluating the flight-test performance of the Tetrad INS. These static laboratory test results are presented in table 13. The principal objective of these tests was to determine if the length of alignment time materially improved navigation performance. A second objective was to measure the static navigation errors. The data in table 13 show the final velocity error (the velocity should always be zero in a static laboratory test), for various alignment times ranging up to 10 min.

Final-velocity error was not systematically affected by alignment time if a stable heading had been computed, which usually took up to 2 min under static conditions. Figure 21 shows the computed estimated heading during alignment (gyro compassing) for six of the static tests shown in table 13 as a function of alignment time. Clearly, the heading angle has been determined within 2 min and sometimes in less than 1 min. External disturbance to the Tetrad during alignment requires additional time for correction. Some of the scatter in figure 17 may be due to disturbances that occurred after alignment was initiated.

In 1977 and 1980 both static and dynamic laboratory tests of the Tetrad were conducted to detect any change in its performance. The results of these laboratory tests which included exposure to 1 to 10-Hz sinusoidal motion on the motion simulator facility and a 2-yr summary are presented in table 14. A comparison of the apparent navigation errors between tables 13 and 14 shows no statistically significant difference between the final velocity of the two sets of test results.

Failure-Detection Test Results

Although the software in the Tetrad's navigation computer included provision for simulating sensor failure on-line, most of the testing of the failure-detection strategy involved the use of flight and laboratory test data in an off-line mode. Raw sensor data were prerecorded and used in a computer simulation of the Tetrad system. The error-detection time (number of data frames) required to detect a simulated step-bias error of different sizes is presented in table 15 for an orthogonal

sensing axis and in table 16 for an ortho-skew sensing axis. (Although each sensor has essentially the same scale factor, a given sensing error in the ortho-skew axis perturbs the parity-residual by a factor of $\sqrt{3}$ more than the same error in an orthogonal axis.) The size of the simulated step-bias errors varied between 10 counts (1.57 arc seconds per count) and 1000 counts. Four different prerecorded samples of test data were used; three of the samples included (1) stationary (constant attitude, no local acceleration); (2) single-axis, 0.1-Hz sinusoidal motion (which appears as a saw-tooth input for the test case selected); and (3) two-axes, 2-Hz sinusoidal motion on the pitch/roll orthogonal axes. A fourth sample consisted of UH-1H helicopter flight-test data exhibiting strong harmonic vibrations, at twice the rotor speed, centered at about 10.5 Hz on all axes (see appendix A).

A single-count error (1.57 arc seconds) occurring in every data frame (sampled at 40 Hz) is equivalent to an error drift rate of 64°/hr. This would be a catastrophic error for navigational use if it persisted but would be negligible for flight control use. The gyro parity-residual error (with no sensor failures) from tables 4-12 experienced during all 4 yr of flight test was bounded by approximately 4 counts. Large (2-3 count) residuals were usually followed on the next data frame by a similar-sized residual of opposite sign. The detection threshold must be set large enough to avoid false alarms or compensating pairs of large errors. If one were to set the threshold at 8 counts and accumulate (integrate) the parity-residual, a gyro error of 0.01°/hr would require about 19 min to detect. During the flight-test periods, the parity-residual for both the laser gyros and the accelerometers was used to monitor the operational states of the navigation system and to determine when the equipment malfunctioned. The parity-residual for the accelerometer was not studied extensively because the navigational errors are more sensitive to attitude errors than to acceleration errors.

Calibration Stability Results

One of the objectives of the flight-test program was to evaluate long-term calibration stability of the individual laser gyros. The accelerometers were not evaluated because the units used in the Tetrad are more advanced instruments relative to the laser gyro, and navigational errors are more sensitive to attitude rate errors than accelerometer bias errors. An effort was made to detect scale-factor and gyro-bias shifts which would indicate a need for recalibration in each laboratory and flight test. An analysis of the test data in the fall of 1977 and contractor-supplied data indicated a possible calibration problem arising from the laser-gyro mounting screws. This was corrected by refastening each laser gyro with proper screws and then executing a program to recalibrate the bias, scale factor, and misalignment coefficients of the laser gyros (and also the accelerometer) in the spring of 1978. The gyro biases can be checked easily by static drift tests. The scale factors and misalignment coefficients require a complex calibration procedure which was provided by Honeywell. It consisted of a series of rotations around each axis, a short alignment, and then 30 sec of navigation to measure simulated incremental velocities (errors). The measured incremental velocities provided a measure of convergence of the iteration and also the new input data for the next iteration calculation of misalignment and scale-factor estimates. This iterative calibration procedure is described in reference 9. Unfortunately, the computational results did not show satisfactory convergence because the uncompensated errors in the incremental velocities were too large. Table 17 shows the effects of uncompensated errors on the measured incremental velocities for five identical samples. For iterative convergence to be successful, the sample-to-sample variation should not exceed 5%. The Tetrad Lab data in figure 21 are typical, but not sufficiently stable to be used for calibration,

because it varied by more than 5%. For these reasons the original Honeywell scale-factor and misalignment values were used but with newer, corrected laser-gyro bias compensation.

During the first 10 mo of operations, Tetrad demonstrated navigational accuracy consistent with its factory specifications of 1-2 knots drift error and no discernible deterioration occurred in its performance. The original gyro-bias compensations are shown in table 18, which shows an unusually large x-gyro compensation of 0.16198°/hr as compared with the 0.046°/hr average for the other three. The required gyro-bias compensations after the remounting are also shown in table 18. These values were used for the remainder of the test program in which the Tetrad continued to perform within its original specifications. The net effect of the remounting was to reduce the excessive x-gyro-bias compensation and change the others without affecting the long-term calibration stability.

CONCLUSIONS

The Tetrad INS performed within the design-specified accuracy range of 1-3 knots error growth, achieving a mean error growth of 1.96 knots, with a standard deviation of ±1.09 knots overall. This is the first flight demonstration of user-acceptable inertial navigation accuracy from a strap-down INS in helicopter operations, and it was achieved with practical alignment times of 5 min or less. The vibration at about 10.5 Hz created by rotor dynamics did not seriously affect navigational performance.

Failure detection using the parity-residual from four axes was successful for failure levels less than 100°/hr, which is generally smaller than the threshold of most flight-control sensing requirements (angular rate sensors with sensing thresholds greater than 1000°/hr are commonly used in flight control systems). The vibrational environment of the helicopter does not seriously affect sensor-failure detection, but must be accommodated if predictive methods of failure identification are to be successful.

During the 4 yr of flight and laboratory testing of the Tetrad no significant changes were required in the laser-gyro initial scale factor and sensor bias calibration although numerous efforts were made during laboratory calibrations to identify any significant shifts.

APPENDIX A

FACILITY-BASED SOFTWARE SYSTEMS FOR FLIGHT-TEST DATA EVALUATION

Test Data Recording

All test data for the Ames Tetrad INS were recorded on a nine-track digital tape. Recorded Tetrad data always included the Tetrad's estimates of position, velocity, and attitude, as well as time, mode flags, bit-correcting codes, etc. It also usually included measured DME ranges, station identification, and time-code information. These "slow" data were recorded at about 1 sample per second. High-frequency (e.g., 40-Hz) samples of inertial sensor (e.g., laser-gyro) data were sometimes recorded as well. The amount of data which could be recorded on any one flight was limited by the length of the tape, capacity of the tape recorder, and the speed of the Tetrad (H301) computer. When high-frequency data were recorded, they were recorded only for a 20-min interval near the beginning of navigation.

The Tetrad INS calculates attitude and navigation information from inertial sensor data sampled at 160 Hz. There are eight 16-bit words per sample, which translates to 2560 characters (8-bit bytes) per second. The Tetrad tape recorder's continuous recording rate is 1250 characters per second, including time required to write record gaps (about 50-75 msec for each gap).

The Tetrad's primary update frequency (160 Hz sampling is for attitude-coning compensation) is 40 Hz. The recording system can accommodate the 40-Hz rate for eight inertial sensor raw data sums plus 64 words of attitude and navigation data at 1 Hz. In this mode, one 600-ft Tetrad tape can hold data for about 30 min of testing. Without recording the 40-Hz data, the same size tape can hold data for about 6 hr of testing. An alternative mode using a scheduled, variable recording rate enables collection of high-rate data during critical test segments, yet maintains a capability for monitoring low-rate data throughout a test. In this mode, both the number and the sampling rate of fast variables can be specified with the input rate schedule.

Flight-Test Data Reduction

Most of the Tetrad postflight data reduction was performed on the CDC 7600 computer at Ames Research Center's central computer facility, although some data reduction was executed in the IBM 360/67, as well as in the H316 computer in the Motion Simulator Laboratory. Figure 22 illustrates the data-reduction process for Tetrad test analysis. Programs are shown as rectangles and disk-files as ellipses in this figure. A flight tape may be processed first on the H316 Quick-Look program. This program prints (tabulates) either low-frequency or 1-Hz data from the tape and provides an optional hexadecimal data dump which is useful for gross assessment of the test results and for verifying that the tape really contains good test data. The H316 computer was also used to make copies of the flight tape for subsequent use on the CDC 7600 because the H316's tape recorder interface is much more tolerant of on-board-recorder tape faults than is the CDC 7600 facility.

As shown in figure 22, the test tape data are first processed by FLTST (the first program in the CDC 7600 sequence of analytical programs). This program decodes and scales the recorded data, tabulates the navigation performance, aircraft attitude,

and range data, and then produces two disk files, STATE and FAST, which are reduced data for use by other programs in the sequence. STATE contains the following low-frequency data: navigation estimates, aircraft attitude, and measured range from the DME. FAST contains the high-frequency laser-gyro and accelerometer sensor data.

Three auxiliary programs use the STATE file. YPRGRF produces plots of northward velocity, eastward velocity, altitude, yaw, pitch, and roll. Figures 23 and 24 are example outputs from this program. LLPLOT produces ground-track plots of a trajectory such as that shown in figure 25. It can plot either the trajectory as estimated by the Tetrad (from STATE) or the trajectory from another reference (e.g., from the DME file), as seen in figure 26. Program DMETOO computes a reference trajectory (the DME file) from the DME ranges that it reads from the STATE file. This program also reads the Tetrad's estimated trajectory from the STATE file and computes position residuals (errors) as functions of time. These are plotted by DMETOO, as shown in figure 27. Position errors computed by DMETT are sampled and used as input to program GTONYK, which resides in the IBM 360/67. This program uses a simple inertial-system error model to estimate the gyro drifts and tilt errors which may have caused the observed position error history. It is also the source of the stated values for navigational error growth (i.e., x knots). Figure 28 illustrates navigational-error modeling results.

Two programs process high-frequency data from the FAST file. MYGRAF plots the laser gyro and accelerometer sensor data, and it computes and plots the parity-residual from the Tetrad's redundant sensor system. An example of MYGRAF's plots is shown as figure 29. Program FOOREA computes and plots the fast Fourier transform (FFT) of a segment of Tetrad sensor data. The FFT develops the spectral power of a signal as a function of the signal frequency. Figure 30 shows a plot of a segment of pitch-gyro data and its spectral density. This figure identifies the predominance of the 10.5-Hz 2/rev oscillation which is always present during UH-1H helicopter flights.

Navigational Data Error Analysis

The tilt-drift error model used to evaluate the performance of the Tetrad system is based on modeling the horizontal (northerly and easterly) velocity and position errors as functions of steady gyro-drift rate compensation errors, tilt (or, equivalently, accelerometer bias) errors, and heading errors. The best estimate of the tilt, drift, and heading errors is made from the multiply redundant position and velocity error data by a least-squares-fit algorithm.

Tilt-Drift Error Model

The one-dimensional linearized differential equations of motion for errors in an inertial navigator are given by equation (A1). The coordinate system is shown in figure 31:

$$\dot{\tilde{v}} = +g\tilde{\theta}_a + \tilde{a}_o \qquad \text{(A1)}$$

$$\dot{\tilde{\theta}} = -\tilde{v}/R + \tilde{\omega} \qquad \text{(A2)}$$

where

$\tilde{v}$ horizontal velocity error

$\tilde{\theta}$ tilt-angle error (from horizontal)

$\tilde{a}_o$ accelerometer-bias error (horizontal)

$\tilde{\omega}_o$ drift-rate bias error (horizontal)

g,R gravity and Earth's radius

Upon integration of the simultaneous differential equations (A1) and (A2), the one-dimensional error model becomes

$$\tilde{v} = -\tilde{\omega}_o R(1 - \cos \omega_s t) \qquad \text{(steady drift and heading)}$$

$$-\left(\tilde{\theta}_o - \frac{\tilde{a}}{g}\right) R\omega_s \sin \omega_s t \qquad \text{(tilt)} \tag{A3}$$

Here ω_s is the Schuler frequency, given by $\sqrt{g/R}$. We have here neglected terms dependent on vertical gyro drift or initial velocity errors.

Least-Squares-Fit Algorithm

Using equation (A3), velocity-error measurements v, at time t_i may be modeled in the form

$$\tilde{v}(t_i) = V_{i1}V_{i2}(\tilde{\omega}_o\tilde{\theta}_o)^T \tag{A4}$$

where

$$V_{i1} = -R(1 - \cos \omega_s t)$$

$$V_{i2} = -R\omega_s \sin \omega_s t$$

Similarly, integration of the velocity equation (A3) gives us

$$x(t_i) = X_{i1}X_{i2}(\tilde{\omega}_o\tilde{\theta}_o)^T \tag{A5}$$

For the position error we have

$$X_{i1} = \frac{-R}{\omega_s}(\omega_s t_i - \sin \omega_s t_i)$$

$$X_{i2} = R(\cos \omega_s t_i - 1)$$

From these observations, we have a set of linear equations error model of the form

$$\left.\begin{aligned} \tilde{v} &= Vd \quad \text{(for velocity errors)} \\ \tilde{x} &= Xd \quad \text{(for position errors)} \end{aligned}\right\} \tag{A6}$$

where

$$d = (\tilde{\omega}_o \tilde{\theta}_o)^T$$

is the unknown drift-parameter vector. The V and X terms are the $N \times 2$ model matrices transforming the 2×1 drift-parameter error vector d into the $N \times 1$ measurement error vectors, $\tilde{v}$ and $\tilde{x}$.

If the number of measurements N exceeds two, N is greater than the number of drift parameters; a least-squares analysis then gives a best-fit drift-parameter vector. Thus,

$$\hat{d} = G_x \tilde{x} \tag{A7}$$

or

$$\hat{d} = G_v \tilde{v}$$

where

$$G_x = \underset{(2 \times 2)}{X^T X^{-1}} \underset{(2 \times N)}{X^T}$$

and

$$G_v = V^T V^{-1} V^T$$

The uncertainty in the least-squares estimate of d is given by

$$\sigma_d^2 = G_X \sigma_x^2 G_X^T$$

$$(2 \times 2)$$

$$= G_V \sigma_v^2 G_V^T \tag{A8}$$

where

$$\underset{(N \times N)}{\sigma_x^2} = \frac{1}{N-1} \underbrace{(\tilde{x} - \hat{x})^T (\tilde{x} - \hat{x})}_{\text{scalar}} I_{N \times N}$$

and

$$\sigma_v^2 = \frac{1}{N-1} (\tilde{v} - \hat{v})^T (\tilde{v} - \hat{v}) I_{N \times N}$$

where $\hat{x}$ and $\hat{v}$ are position and velocity estimates obtained from the tilt-drift error model applied to the least-squares fit for the drift parameters; $I_{N \times N}$ is the $N \times N$ identity matrix. The assumption has been made that measurement errors at two different time points are uncorrelated and have the same distribution.

In the Tetrad system, horizontal gyro data are obtained from orthogonally placed instruments which define the x and y body axes. These data are referenced to north and east axes as illustrated in figure 31. Estimates are then obtained for the north and east drift-rate-bias errors. Positive values of $(\hat{\tilde{\omega}}_o)_{east}$ result in negative values of $\tilde{v}_n$, and positive values of $(\hat{\tilde{\omega}}_o)_{north}$ result in positive values of $\tilde{v}_e$. One may then obtain the navigational error growth from

$$\hat{\tilde{v}}_{mean} = (60 \text{ n. mi./deg}) \cdot (\hat{\tilde{\omega}}_{on}^2 + \hat{\tilde{\omega}}_{oe}^2)^{1/2}$$

with both components of ω_o measured in degrees per hour.

Up to six DME range values are used to obtain values for $\tilde{x}_n$ and $\tilde{\omega}_e$ during flight tests, where

$$\tilde{x} = X_{Tetrad} - X_{DME}$$

During static (laboratory) tests, the true velocity is zero, which equates the velocity-error data to the measured v.

APPENDIX B

PARITY-RESIDUAL SENSOR-FAILURE DETECTION ALGORITHM

Symbol and Variable Conventions

The Tetrad reference frame is orthogonal and corresponds to the edges of the box containing the Tetrad instrument package. The orthogonal sensor's input axes are (neglecting misalignments) parallel to the axes of the Tetrad reference frame. The transformation of coordinates to the Tetrad frame from the current body reference frame, in which the Tetrad instrument package is mounted, will be denoted ${}_{t}T^{D}$.

Let u_i represent a unit vector along the input axis of the ith sensor. This vector will be denoted ${}_{t}u_i$ when it is expressed in Tetrad frame components and ${}_{b}u_i$ in the body frame (${}_{b}u_i = {}_{b}T^{t}\ {}_{t}u_i$). The Tetrad frame components of the four sensor axes are denoted by the 3×4 matrix ${}_{t}U$.

$$ {}_{t}U = ({}_{t}u_1\ {}_{t}u_2\ {}_{t}u_3\ {}_{t}u_4) = \begin{pmatrix} 1 & 0 & 0 & \cos\eta \\ 0 & 1 & 0 & \cos\eta \\ 0 & 0 & 1 & \cos\eta \end{pmatrix} \tag{B1} $$

The right-most terms are true for the ortho-skew configuration. The angle η is the angle between the skewed sensor's (sensor No. 4) input axis and the axes of each of the orthogonal sensors. The body-frame components of the four sensor axes are

$$ {}_{b}U = ({}_{b}u_1\ {}_{b}u_2\ {}_{b}u_3\ {}_{b}u_4) = {}_{b}T^{t}\ {}_{t}u \tag{B2} $$

The sensing-axis unit vectors can be written as a linear combination of the other three. In particular,

$$ u_4 = \alpha v_1 + \beta v_2 + \gamma v_3 \tag{B3} $$

Measurement Model

The sensors modeled in this paper are of the integrating type so that the output measurement is the integral of the sensed input over the sampling time interval, Δ.

A gyro whose sensing axis is u_i senses the component of the angular velocity Ω which lies along u_i. More generally, the gyro's measured output is a scaled version of $u_i\Omega$ which includes bias, quantization, and other effects. The gyro-measurement model adopted for this paper is

$$ \Delta\theta_i(t) = \left\{ \int_{t-\Delta}^{t} (b_i + S_i\Omega)d_t + \tilde{q}_i + \tilde{r}_i \right\} \tag{B4} $$

In these equations, the notation "{ }" means "integer part of," b_i is bias, S_i is the laser-gyro's scale factor and compensation vector, $\tilde{q}$ is a quantization error, and $\tilde{r}_i$ is random error. The quantities b_i and S_i are estimated for each sensor

from their calibration data. The four gyro outputs are then used to compute the estimated Ω. The generic notation is used in this paper, where m_i is the estimated output of the ith sensor for phenomenological input vector p.

The equation

$$m_i = u_L \int p d\tau \tag{B5}$$

illustrates, approximately, the relationship between the input (p) and the sensor's output (m_i).

Transformation to Orthogonal Triad Reference Coordinates

For aircraft sensor measurements to be useful in aircraft guidance and navigation, they must first be transformed from the Tetrad reference frame into equivalent orthogonal triad components relative to the aircraft body reference frame. A least-squares procedure is used in the transformation.

Failure Detection by Parity-Residual Sum Divergence

A relationship exists for any Tetrad configuration that relates the measurements from the four like sensors.

$$m_4 = \alpha m_1 + \beta m_2 + \gamma m_3 \tag{B6}$$

Equation (B6), which follows from equations (B3) and (B5), states that the output of any sensor can be formulated as a linear combination of the outputs of the other three sensors. This relationship is called parity, and the coefficients α, β, and γ are called parity coefficients. They can be determined from the Tetrad's geometrical configuration. For the ortho-skew configuration,

$$\alpha = \beta = \gamma = \cos \eta = 1/(3)^{1/2} \tag{B7}$$

More generally,

$$\begin{pmatrix} \alpha \\ \beta \\ \gamma \end{pmatrix} = (\hat{u}_1 \ \hat{u}_2 \ \hat{u}_3)^{-1} \ \hat{u}_4 \tag{B8}$$

Equation (B6) never strictly holds in practice, hence a Tetrad parity-residual, ε_s, is defined as follows:

$$\varepsilon_s = m_4 - \alpha m_1 - \beta m_2 - \gamma m_3 \tag{B9}$$

Thus, ε_s is the difference between the observed m_4 and the m_4 computed in equation (B6). For a perfect system, ε_s would always be zero in the absence of failures. Normal instrument errors and output quantization cause the parity-residual to take on a small range of values in normal operation. When a failure occurs, the parity-residual exceeds its normal range. Thus, single failures can be detected by monitoring ε_s. In this study, the parity-residual is summed over a specified number of

sequential data frames in order to detect small but persistent failures. These sequential data frames are collectively called the "accumulation interval for detection" or the "detection window," and they are denoted by τ_d. The detection threshold d is the tolerance on the parity sum. A failure is indicated when the magnitude of the parity sum exceeds the detection threshold. This failure condition is

$$\left| \sum^{\tau_d} \varepsilon_s \geq d \right| \tag{B10}$$

The detection threshold and the length of the detection window determine the level of step failure that can be detected.

The parity coefficients are computed from the best estimates of the orientations of the sensors, but the measurements will be made by the sensors in their actual orientations. The differences between the estimated and actual orientations are misalignment errors. The coefficients, computed as in equation (B7), depend on the orientations of all four sensors even though the coefficients multiply only three measurements in the parity-residual. A bias-compensation error affects the parity-residual in proportion to the coefficient it multiplies. That is, a bias error in sensor No. 4 contributes to the parity-residual directly, and a bias error $\tilde{b}$ in sensor No. 3 contributes $-\gamma\tilde{b}$ to the parity-residual. Thus, for the ortho-skew configuration, a bias error of one unit in sensor No. 4 is equivalent to a bias error of $(3)^{1/2}$ units in any one of the other three sensors in its effect on the parity-residual. Therefore, biases and scale-factor compensation errors can cause false alarms. Random-measurement errors, which have small means and variances relative to the quantization level, will not significantly affect the parity sum.

Failure detection in a Tetrad inertial sensor unit is a simple operation of calculating the parity sum from accumulation of the parity-residual. When the magnitude of the parity-residual sum exceeds the present detection threshold, a failure is indicated. The minimum level of step-error that can be detected is determined by the number of points in the parity-residual sum and the size of the detection threshold.

The apparent time frame of failure can be inferred by summing the parity-residual backward from the time of failure detection until this sum exceeds a preset threshold level. This procedure is illustrated in figure 7, with a moving window integration, and in figure 8, which illustrates how the failure time is estimated from the parity sum and the preset threshold. This preset threshold is determined from the dynamic characteristics of the Tetrad system and is influenced by uncompensated bias and scale factors, as well as by the sensor quantization.

APPENDIX C

TETRAD DUAL-COMPUTER SYSTEM

DUAL-COMPUTER ORGANIZATION

The Tetrad system's airborne software includes programs for its two processors, CPU No. 1 and CPU No. 2. CPU No. 1 is the system navigation computer. It receives inertial sensor data and baro-altimeter data, performs compensation for sensor anomalies, performs failure-detection and isolation calculations, controls the control/display unit (CDU), and computes the navigation and attitude estimates. Basic navigation software for CPU No. 1 was developed by Honeywell, Inc. Analytical Mechanics Associates, Inc. (AMA) has been the principal developer of CPU No. 2 software. CPU No. 2 is primarily concerned with collecting and tape recording test data. The dual-computer system's data flow is illustrated in figure 32.

CPU NO. 1: SYSTEM NAVIGATION COMPUTER

Machine language software provided with the NASA Ames Tetrad INS executes strapdown, skewed redundant inertial computations in the navigation computer for the navigate and alignment modes of system operation. Figures 33 and 34 depict the major software functional blocks for the navigation and alignment modes identifying major signal flow paths and approximate execution rates.

Navigate-Mode Software

The navigation-mode software operates on the input words from the skewed Tetrad ISA sensor pulse sample counters to compute and output aircraft latitude and longitude; velocity-track-angle and ground speed; roll, pitch, and heading angles; roll, pitch, and yaw angular rates; and longitudinal, lateral, and lift acceleration. As observed in figure 33, the basic computational operations used to develop these output signals can be grouped into five categories: sensor-signal compensation, redundancy management, attitude compensation, position/velocity update, and output computations.

Sensor signal compensation— Sensor-signal compensation includes gyro input channel compensation, quantization, accelerometer input channel compensation, and size effect compensation.

Gyro input channel compensation. Known systematic errors are present on the input signals from each gyro as a result of manufacturing tolerances and small startup and thermal sensitivities. They are measured for each gyro, and the associated error coefficients stored in the navigational computer memory for correction during system operations. Gyro systematic errors accounted for in the system software are fixed bias, scale-factor error, misalignment errors, initial startup transient, and bias thermal coefficient. In computing scale-factor error corrections, orthogonal computed rate data are utilized from the previous computational cycle.

Quantization compensation. Because of readout logic and quantization of output data from the laser gyro in pulse-incremental form, rotation data that are not large

enough to trigger an output pulse can be stored in each gyro. Under a rate input in a given direction, a systematic error exists on the accumulated gyro output signal as a result of this effect. The quantization compensation computation corrects this error as a function of the change in sign of the rotation data measured from each gyro.

Accelerometer input channel compensation. Systematic bias, scale-factor error, scale-factor thermal coefficient, and misalignment errors for each accelerometer are corrected by this software element. Scale-factor error corrections utilize orthogonal acceleration data generated during the previous computation interval.

Size-effect compensation. Because of the finite size of the accelerometer assembly in the Tetrad ISA, each accelerometer measures a component of acceleration of a slightly different physical point. In a nonrotating acceleration environment, no error would be created by this effect because all points in the ISA would undergo equal accelerations. In a rotating environment, however, the acceleration of each point in the ISA would differ according to its relative vector position location and the imposed angular velocity vector. The size-effect-compensation block computes a correction for this phenomenon, using orthogonal rate information from the previous computation interval combined with known accelerometer assembly geometry data.

Skewed-sensor redundancy management— Skewed-sensor redundancy management includes simulated gyro-failure computation, skewed-gyro voting logic, orthogonal rotation increment computation, simulated accelerometer failure computations, skewed-accelerometer voting logic, and orthogonal velocity increment computation.

Simulated gyro failure. Any one of the four gyros can be selected to simulate failure through the simulated gyro-failure computation. Failure types that are simulated in this subroutine include bias shift, scale-factor shift, opens, and hard-overs of any magnitude from the limits of the gyro performance specification to its full output capability. The particular failure mode (composite of the latter effects) to be simulated is established by putting constants with prescribed values into the navigation computer from the SSEU. The computed (simulated) failure-mode signal is then used in place of the actual gyro input signal in subsequent software computation. The particular gyro (of the four) that has its signal corrupted is controlled by the CDU.

Skewed-gyro voting logic. The skewed-gyro voting logic compares the compensated signals from the four gyros (including the gyro with the simulated failure) to determine if a failure has occurred. Upon detecting the occurrence of a failure, a discrete is issued to light the CDU gyro-failure-detected lamp. Simultaneously, the discrete is issued to the orthogonal-rotation-increment-computation subroutine to "switch out" the failed gyro and revert to three-gyro operation. The voting logic for failure detection is for the square of the integrated weighted sum of the four gyro signals to exceed a quadratic time function. Particular coefficients in the quadratic equation represent quantization, random walk, and fixed bias error uncertainties, which can be selected by CDU input to the navigation computer.

Orthogonal-rotation-increment computation. Data from the four skewed gyros (or three if a failure has been detected by the skewed voting logic) are combined in this computational element to derive the equivalent orthogonal (roll, pitch, yaw) data. If four gyros are being used, the skew to orthogonal transformation includes a statistical averaging. If three gyros are being used (after a detected simulated failure), the transformation to orthogonal components is a direct 3×3 matrix operation.

The orthogonal rotation increments are actually computed twice, once in double-precision from compensated sensor signals (at 40 Hz), and once in single-precision from uncompensated sensor signals (at 160 Hz). The double-precision signal is used for the critical attitude-update computation. The single-precision signal is used to compute coning compensation, a small correction term for which single-precision arithmetic has sufficient accuracy. Both computations use gyro data signals, the accuracy of which has first been verified by the skewed voting logic.

Simulated accelerometer failure. Operation of this block is analogous to the equivalent gyro block. Failure-simulation capabilities include accelerometer bias, scale-factor error, opens, and hard-overs over the range from the performance specification limits to the maximum output capability of the instrument.

Skewed-accelerometer voting logic. Operation of this block parallels that for the gyros. As with the gyro voter, when the occurrence of an accelerometer failure has been detected, discretes are simultaneously issued to the orthogonal velocity increment computation block, and to the CDU to light the accelerometer failure detected lamp.

Orthogonal-velocity-increment computation. The computation in this subroutine directly parallels the equivalent block for the gyros. For the accelerometers, only a single-precision output is needed.

Attitude computation- The attitude-computation function consists of four elements: direction cosine update, coning compensation, rotation of local vertical frame, and orthogonalization.

Direction cosine update. The basic inertial attitude information in the navigation computer is computed in the form of a fourth-order, direction-cosine updating algorithm. The algorithm is a direct Taylor series expansion of the classical exact-direction cosine change over the updating interval for a three-axis rotation about a fixed spatial axis (zero coning). The direction cosines are updated in double-precision to minimize the effect of computer round-off error drift. To reduce the computational load, only two rows of the direction-cosine matrix are updated with the above updating algorithm. The third row is computed in single precision from the cross-product of the other two rows.

Coning compensation. The coning-compensation algorithm corrects the zero-coning assumption implicit in the direction-cosine update (i.e., nonrotation of the aircraft angular velocity vector over the direction-cosine update interval). The coning-compensation algorithm operates on input data samples taken at 3 times the direction-cosine update frequency to compute an adjustment to the incremental orthogonal rotation data such that when operated upon by the direction-cosine algorithm, an update will result that corresponds to the true direction-cosine attitude change in the actual coning environment.

Rotation of local vertical frame. The direction cosines in the navigation computer represent the attitude of the aircraft relative to locally vertical coordinates. Consequently, the direction-cosine matrix requires periodic updates to account for inertial rotation of the local vertical due to Earth's rotation and aircraft translational motion over Earth's surface. The rotation-of-local-vertical-frame computation block updates the direction-cosine matrix for Earth rate (determined from local position data, using an ellipsoidal Earth model) and aircraft velocity, using a first-order updating algorithm.

Orthogonalization. To prevent any residual errors in the direction-cosine updating process from causing magnitude divergence (from unity) and attitude divergence (from orthogonality) in the cosine vectors, an orthogonalization algorithm is applied periodically to the two direction-cosine vectors being updated. The direction-cosine update software is designed to preclude the need for orthogonalization correction. The orthogonalization correction is only included in the software package as a safeguard against unanticipated residual drifts.

Position-velocity update— The position-velocity update function is composed of the following computational blocks: velocity accumulation in local vertical frame, rotation compensation, Coriolis and gravity compensation, altitude stabilization, and position computation.

Velocity accumulation in local vertical frame. This computation block sums the contributors to the total aircraft-velocity-change vector in local-vertical navigation coordinates to update the estimate of aircraft velocity relative to Earth. Navigation coordinates use a geodetic vertical and an azimuthal wander implementation to avoid incurring permanent errors in the position and velocity information in flights over Earth's north or south poles owing to analytical singularities in Earth latitude and longitude coordinates. The total velocity-change vector processed by this algorithm is composed of accelerometer-derived signals (including compensation), gravity effects, and Coriolis effects. The accelerometer-derived velocity-change increment is calculated by transforming the signals from the accelerometer channel through the direction-cosine matrix relating aircraft (accelerometer) axes to local-vertical navigation coordinates.

Rotation compensation. The transformation of the accelerometer-derived velocity increments through the transformation matrix presumes that the velocity increments were created by an instantaneous acceleration impulse at the time frame of direction-cosine update. The accumulation of the velocity increments actually occurs smoothly over the interval between direction-cosine updates. The rotation-compensation algorithm computes a correction term for this effect, which, when added to the accelerometer-derived velocity increments, produces the correct result upon transformation through the direction-cosine matrix.

Coriolis and gravity compensation. The vertical-velocity change caused by gravity is computed in this block (horizontal gravity-acceleration components are equated to zero, consistent with the geodetic vertical navigation coordinate frame implementation). The Coriolis velocity change computed in this block is a kinematic effect needed to compensate for apparent accelerations in the rotating local-vertical navigation coordinate frame.

Attitude stabilization. The vertical channel of a pure inertial navigation computation is unstable because of the error characteristics of vertical position uncertainties propagating through the gravity model. In this computational block, a third-order blending filter is used to mix barometric altitude with inertially derived vertical-velocity incremental data to limit altitude errors and produce an accurate estimate of vertical-velocity changes.

Position computation. Velocity information is combined in this block with Earth rate-component data (from calculated aircraft position) to derive the local vertical-rate data needed in the rotation of local-vertical frame computation block. Velocity data are also used in this block to compute the angular rate of the navigation coordinate frame relative to Earth. These angular-rate data are then used to update a set of direction cosines relating navigation coordinates to Earth-fixed coordinates.

The angles between these coordinate frames define the aircraft's position over Earth. The position computation block derives aircraft position information in terms of latitude and longitude for output from these latter cosines. A secondary output from this computation block is the wander angle (between local north and the azimuth-wander navigation coordinate horizontal x-axis).

Output computations— The output computations are composed of velocity computation, Euler angle computation, angular-rate computation, linear acceleration computation, and position computation.

Velocity computation. The velocity-computation block uses the wander-angle signal from the position-computation block to convert velocity-vector data in navigation coordinates to ground speed and track angle (angle between the velocity vector ground projection and north). This computational block also provides the I/O software interface function needed to output these data from the navigation computer.

Euler angle computation. The Euler-angle computation block converts the direction-cosine update block attitude data into sines and cosines of roll, pitch, and heading Euler angles relating aircraft axes to local north, east, and vertical coordinates. The wander-angle signal from the position-computation block is used in this calculation to relate azimuth-wander navigation coordinates (direction cosine reference) to north. Included in the computation block are the software calculations necessary to output the data in the required I/O format from the navigation computer.

Angular rate computation. This calculation provides the software interface with the navigation computer I/O for roll-, pitch-, and yaw-rate signal outputs. These signals are directly proportional to the orthogonal rotation increment data used to update the direction-cosine matrix.

Linear acceleration computation. This calculation provides the software interface with the navigation computer I/O for lift, longitudinal, and lateral acceleration signal outputs. These signals are directly proportional to the orthogonal velocity-increment data used in the inertial-velocity accumulation algorithm.

Position computation. In addition to the computations described in the previous subsection, the position computation block provides the software interface with the navigation computer I/O for latitude and longitude outputs.

Alignment-Mode Software

The alignment-mode software operates on the input words from the skewed Tetrad ISA sensor pulse sample counters to compute the attitude of the aircraft (ISA) relative to local north, east, and vertical coordinates for initialization of the navigate-mode direction cosines. Shown in figure 34 is the basic computational operations used to develop these alignment data. These operations can be grouped into six categories: sensor-signal compensation, skewed-sensor redundancy management, attitude computation, alignment-error measurement, initial alignment estimate, and navigate-mode initialization.

Sensor-signal computation— These operations are nearly identical to those performed in the navigate mode, the only difference being a 50% reduction in the iteration rate (to 20 Hz).

Skewed-sensor redundancy management— These operations are also nearly identical to those performed in the navigate mode. The only difference is a 50% reduction in the iteration rate of the 40-Hz computation blocks (to 20 Hz).

Attitude computation— These operations are the same as those performed in the navigate mode with three exceptions: the direction cosines are initialized at unity, the rotation of the local-vertical frame computation is eliminated, and the iteration rate for the 40-Hz computation blocks is reduced by 50% (to 20 Hz). The direction cosines resulting from this set of calculations represent the attitude of the ISA relative to its inertial attitude at the instant of alignment mode initiation.

Alignment-error measurement— The alignment-error measurement calculation is composed of four computational blocks: weighted velocity accumulations in initial coordinates, rotation compensation, filter, and level velocity components computation.

Weighted velocity accumulations in initial coordinates. This computation is analogous to the velocity-update calculation during the navigate mode. Velocity increment data derived from the accelerometer readings are transformed through the direction-cosine matrix (into initial coordinates) and summed to determine a velocity vector that does not include the integrated gravitational acceleration component. Two additional vectors are obtained by a similar transforming and summing operation by first applying a time-function weighting factor to the transformed vector components before summation. Two different time functions are used, one for each of the time-weighted velocity vectors being generated.

Rotation compensation. This block serves the same function as its equivalent in the navigate mode. For the alignment mode, it is operated at 50% reduced speed (at 20 Hz).

Filter. The three vectors generated in the weighted velocity accumulations in initial coordinates block are filtered to attenuate higher-frequency aircraft motion signals sensed by the ISA accelerometers (aircraft acceleration noise).

Level velocity components computation. This computation block combines the three weighted velocity-accumulation vectors with current estimates of the initial aircraft vertical attitude (at alignment-mode initiation) and the value of horizontal Earth rate components in the initial aircraft local-vertical coordinate frame to derive two components of aircraft horizontal velocity accumulation. These measurements are identical to what would have resulted from a summation of horizontal velocity increments from alignment-mode initiation using the current estimate of initial attitude and Earth rate components for attitude initialization and to account for Earth rotation during the summation time interval. Since the aircraft is stationary during the alignment-mode computations, these velocity components should be zero. Nonzero values are indications of errors in the estimates of the initial vertical and Earth rate components and form the basis for revisions in these estimates to be incorporated in the next computation cycle.

Initial alignment estimate— These calculations include the computation blocks labeled Kalman error estimate, update initial vertical attitude matrix estimate, and update local level Earth rate components estimate.

Kalman error estimate. The Kalman-error-estimate block applies four time-scheduled gains to the two horizontal velocity component measurements to develop estimates for the errors in the vertical and Earth rate component estimates. The estimation errors represent two initial Euler angle estimation errors (in roll and

pitch from the initial ISA attitude to the local horizontal plane) and two Earth rate component estimation errors (along the axes of the horizontal coordinates corresponding to the outcome of the latter initial roll, pitch sequence). The scheduled gains used in this calculation are precomputed, optimal, Kalman estimator time-scheduled gains stored in the software memory. The gains are designed to provide optimal error estimates in the presence of anticipated statistical variations in the velocity measurements caused by initial startup alignment uncertainties, aircraft acceleration disturbances caused by wind-gust loading through the airframe and landing-gear structure, gyro quantization noise and random walk, and accelerometer quantization.

Update initial vertical attitude matrix estimate. This computation block updates the estimate of the two initial Euler angles relating ISA initial attitude to the horizontal, and computes a corresponding direction-cosine matrix from the updated angle data. The resulting new estimate for the initial vertical attitude matrix is then fed back to the level velocity components computation block for the next iteration error measurement and update.

Update local level Earth rate components estimate. This block increments the two horizontal Earth rate component estimates by the associated error estimates in these quantities, as determined in the Kalman-error estimate. The revised Earth rate estimates are fed back to the level-velocity-components computation for the next iteration error estimation. The third Earth rate component (the vertical component) is known from known initial latitude. It is, therefore, not a quantity to be estimated as part of the alignment-mode computations.

Navigation-mode initialization— The navigation-mode initialization calculation is performed once at the completion of the alignment-mode period of operation. These computations, performed in the "compute-cosines-of-current-attitude-relative-to-north/local-vertical" block, entail the products of three matrices: the instantaneous cosine matrix from the direction-cosine update block, the final estimate for the initial vertical-attitude matrix, and the direction-cosine matrix relating the initial horizontal coordinate frame in inertial space to the orientation of this frame at the end of the alignment mode, if it had remained fixed to Earth during alignment (i.e., the Earth angle rotation matrix). Since Earth's rate is a constant vector, the final estimated values for the horizontal Earth rate components can be used with the known vertical Earth rate component and alignment time to calculate the latter matrix. The triple-matrix product described above becomes the initial direction-cosine matrix for the navigate mode, relating ISA attitude to local vertical-navigation coordinates at navigate-mode startup. The initial wander angle for the position computation block is also computed in this computation element from the level Earth rate components (compared with the horizontal values along east and north axes, zero and a known function of latitude, respectively).

CPU NO. 2: RESEARCH COMPUTER

The primary function of CPU No. 2 in the Tetrad navigation system is to record test data, most of which is computed in CPU No. 1. It also (1) receives and interprets DME and time-code data; (2) receives gyro status data from the ISA; (3) transmits data to the serial data transmitter; and (4) transmits data to the D/A converter for analog transmission. These functions are quite different from those of CPU No. 1, which has the primary computational load.

The software of CPU No. 2 is charted in figure 35. This software is for the navigational phase of Tetrad research; the CPU No. 2 software for the integrated flight management phase is not shown. The figure shows two interrupts as entries. The "power-recovery" interrupt takes place when the computer is turned on. This interrupt causes the program counter to go to zero and initiates execution there. The "standard" interrupt sets the program counter to 1 and execution takes place from that point. The standard interrupt is sent from CPU No. 1 at approximately 40 Hz during navigation and 20 Hz during alignment. That is, CPU No. 2 is "driven" by CPU No. 1. The interrupt rate is not quite regular, since the time of interrupt depends on completion of a certain set of computations in CPU No. 1, and this may occur irregularly because of differing logical paths in execution. The following steps elaborate on the elements of figure 35.

Initiation

Program initiation takes place at the power-recovery interrupt when the computer is turned on. Parameter values are set for the later recursive execution of the CPU No. 2 program. Execution is then transferred to the wait-loop to await an interrupt from CPU No. 1. If skip-key X5 is set (which can only happen if the SSEU is connected) the utility program is executed. This program enables examination and modification of any memory location in the computer.

Input from CPU No. 1

CPU No. 1 supplies 120 words of data to CPU No. 2 via A-register transfers at every interrupt. The list includes raw data, attitude, navigation results, and time and mode words. The transfer requires approximately 4 msec.

Serial Transfer Variables

A set of 20 word-pairs is formatted for transmission to V/STOLAND. This involves calculation of some derived variables, such as magnetic heading. The navigation tests were all performed without a serial receiver (i.e., without V/STOLAND). Some of the serial transfer variables were recorded on the magnetic tape.

Analog Data

It was originally intended that the Tetrad would send analog signals to STOLAND for flight-control purposes. It was later decided to display heading and altitude on digital voltmeters in flight. The digital voltmeters were also used to display pitch and roll during motion simulator tests. Analog ports were also used to strip-chart interim alignment results during laboratory testing. The words must be scaled and addressed before being sent to the D/A converters.

Parity Calculations

Accelerometer and gyro parity-residuals are among the 120 words provided at 40 Hz by CPU No. 1. CPU No. 2 contains logic to sum these residuals continually and to compute the extrema for a 10-frame window sum.

Raw-Data Sums

Forty-hertz accelerometer and gyro data are summed continually for recording. Recording the sum is preferable to recording the individual samples for two reasons:

1. When there is a bad recording (missing data), the next good sum enables perfect recovery; recording individual samples would result in loss of data.

2. The sum may be sampled at a lower rate (than that at which it was recorded) in postflight reduction or it may be recorded at a lower rate and still contain the same integral information.

Fast Variables

The CPU No. 2 logic includes a capability for selecting up to 16 variables to be recorded at selected rates (submultiples of 40 Hz). A decimation of 2 gives a recording rate of 20 Hz during navigation. This capability was used primarily for recording gyro and accelerometer data during flight. Variables to be recorded are selected from a list of their addresses. A scheduling capability permits automatic changing of the number of fast variables and their output rate based on elapsed time in the navigation mode.

DME and Time Code Data

CPU No. 2 receives DME and time-code data in some dedicated memory locations by DMA transfer from the SCORE receiver. The DME data include range, frequency, and channel number. The information is coded and contains only four bits of usable data per input word. Transmission is considered to be complete when the last DME word contains a specific bit pattern. Logic in CPU No. 2 masks and repacks the relevant bits for compact recording. These data are stored with the 1-Hz output variables. Past and past-past values are also recorded to accommodate the possibility that two or three stations are sampled in a 1-sec interval.

1-Hz Data

A 64-word block of "slow" data is stored away for output every 40 interrupts (approximately 1 Hz in navigation). This block includes latitude, longitude, altitude, velocity, attitude, direction cosines of the level-to-body transformation in double-precision, DME and time-code data, indicators of decimation and number of fast variables to follow, gyro status words, parity-residual sum extrema, and bit-repair data for the other words. The decimation and number indicators are used in postflight processing of the recorded data and are needed because of the capability for automatically changing the output frequency and number of "fast" variables. Eight gyro status words for one gyro are brought into CPU No. 2 every second via an A/D transfer from the ISA. These were supposed to indicate gyro condition status, but have never been found to be meaningful. The bit-repair data are redundant recordings of two specific bits of each recorded word. The two bits have frequently been in error (probably because of faulty line-drivers between CPU No. 2 and the microprocessor which feeds the tape drive). By redundantly recording the bits, the postflight data reduction process can repair the faulty bits. Each bit-repair word contains repair-bits for seven data words, so the 64-word block of 1-Hz data contains 56 data words and 8 bit-repair words.

Output for Recording

The tape-writing logic in CPU No. 2 sends 16 words of data from the output buffer to the microprocessor during each 25-msec interrupt interval. This is done only in those interrupt intervals during which the output buffer has been filled and has not yet been emptied. The logic provides double-buffering, so that one buffer is being filled while the other is being emptied. When a buffer is filled, the roles are switched and the write-flag is set for the just-filled buffer. It is important that CPU No. 2 not be trying to transmit data to the microprocessor when a CPU No. 1 interrupt occurs — hence the limit of 16 words transmitted during each interrupt cycle. Recorded words are complemented and sent to the microprocessor 1 byte at a time. After sending the 16 words, the program jumps to the wait-loop to await interrupt from CPU No. 1.

APPENDIX D

THREE-AXIS MOTION SIMULATOR FACILITY

The Three-Axis Motion Simulator Facility was developed at Ames Research Center for testing inertial sensor hardware components with system concepts applicable to strap-down inertial navigators. The facility includes a three-axis gimballed table which provides attitude and attitude rate simulation; two Honeywell H316 minicomputers; a dual floppy-disk with S100 microcomputer; two 9-track Kennedy digital magnetic tape recorders; a 128-character line printer (300 lines per minute); and other peripherals required for detailed system testing. An adapter plate was built to allow the laser-gyro Tetrad inertial sensor assembly (ISA) to be installed on the motion simulator with ±15° of yaw and pitch-attitude range. The simulator with the laser-gyro ISA and the minicomputer facility is shown in figure 14.

The attitude simulator includes an orthogonal, three-axis, hydraulic-driven gimballed system controlled by an electrohydraulic servo whose attitude inputs have the potential to be derived from V/STOL flight profiles prerecorded on magnetic tape, or by a function generator with sine wave, triangular wave, or ramp outputs at selected frequencies and rates. Monitoring of gimbal angles is accomplished with high-resolution linear inductosyn digital shaft encoders whose angular resolution is 2.5 arc seconds. The table is mounted on a concrete base 1.5 m (5 ft) in depth, which is in turn supported by 30.5-m (100-ft) pilings.

The motion-simulator data acquisition system, schematically shown in figure 16, consists of six time-division multiplexed channels which are used to transmit both digital and analog angular position information from the gimbal axis. The information from the analog encoders is recorded on an analog recording system; the data from the digital shaft encoders are displayed and recorded on a digital magnetic tape recorder. The copies and formatted magnetic tape data can be analyzed by the central computer facility, using the IBM 360 or the CDC 7600 computers at Ames when desired. The data-analysis program in the minicomputer performs the functions of parity-error computation, sensor cumulative count averaging, gyro-error detection, and a comparison of sensor and shaft encoder angular-position information. The output of each program can be displayed on a line printer for quick-look analysis.

Sensor data are first formatted and processed and then transmitted to a Tetrad-mounted digital magnetic tape recorder. The dual H301 computers in the Tetrad flight system provide the data formatting.

The Tetrad's data, after being recorded digitally on magnetic tape, requires no preprocessing or reformatting to be read on the laboratory H316 computers or on the central facility computers. The H316 minicomputer permits rapid review of test data.

REFERENCES

1. Bjorkman, W. S.: Final Report for Development of Aided Inertial System Computer Programs. Analytical Mechanics Associates, Mountain View, Calif., May 1975.

2. Eberlein, A. J.; and Savage, P. G.: Strapdown Cost Trend Study and Forecast. NASA CR-137585, 1975.

3. Eberlein, A. J.; and Lalm, T. G.: Failure Detection and Isolation Investigation for Strapdown Skew Redundant Tetrad Laser Gyro INS. NASA CR-137730, 1976.

4. Sorensen, J. A.; Bjorkman, W. S.; and Kidder, N. M.: A Concept for Tetrad Failure Isolation Using External State Measurements. Report 79-01, Analytical Mechanics Associates, Mountain View, Calif., Jan. 1979.

5. Hruby, R. J.; Bjorkman, W. S.; Schmidt, S. F.; and Carestia, R. A.: A Study of Redundancy Management Strategies for Tetrad Strapdown Systems. NASA TM X-78576, 1979.

6. Hruby, R. J.; Bjorkman, W. S.; and Carestia, R. A.: An Evaluation of Sensor Fault Detection and Identification Algorithms for Improved Utilization of Tetrad Configured INS. Proceedings of the 9th Biennial Guidance and Test Symposium, Holoman AFB, Oct. 1979.

7. Rood, R. J.; Vaughn, D. K.; and Seacord, C. L.: Development of Procedures and Criteria for Analysis of Flight and Laboratory Test Data on RLG Internal Status Signals in Regard to Failure Detectors: Final Report. NASA CR-152400, 1980.

8. Hruby, R. J. et al.: Flight Test Results of Strapdown Hexad Inertial Reference Unit (SIRU). NASA TM X-73224, 1977.

9. Savage, P. G.: A Calibration Procedure for Laser Gyro Strapdown INS. 9th Annual Electro-Optical Conference and Exhibition, Anaheim, Calif., Oct. 25-27, 1977.

10. Bjorkman, W. S.: Final Report for Analytical Support in Tests of the Ames Tetrad in V/STOL Aircraft. Analytical Mechanics Associates, Mountain View, Calif., Jan. 1979.

TABLE 1.- DME STATION LOCATIONS FOR FLIGHT-TEST PROGRAM

DME	Latitude, deg	Longitude, deg	Altitude, ft	Frequency, Hz	Range, n. mi.	Bearing, deg	Acquisition altitude, ft
Modesto	37.62	-120.95	90	108.4	14.70	19.08	242.0
Crows Landing	37.40	-121.11	170	110.2	.45	-158.43	-28.8
Woodside	37.39	-122.28	2270	111.4	56.11	-101.01	651.3
San Francisco	37.61	-122.37	10	111.6	61.68	-88.16	3490.8
Los Banos	36.71	-120.77	2107	112.6	44.72	149.07	-199.4
Fresno	36.88	-119.80	100	112.9	70.08	106.27	4379.0
San Jose	37.36	-121.92	48	114.1	39.42	-104.09	1465.4
Linden	38.07	-121.00	260	114.8	39.95	-2.98	1290.5
Sacramento	38.44	-121.55	5	115.2	65.26	-28.78	3897.3
Friant	37.10	-119.59	2380	115.6	74.81	93.77	2703.6
Stockton	37.83	-121.17	40	116.0	25.37	-16.89	669.5
Oakland	37.72	-122.22	30	116.8	56.42	-80.36	2922.1
Salinas	36.66	-121.60	77	117.8	50.83	-162.05	2346.0
Moffett Field	37.43	-122.05	4	117.6	45.39	-98.36	1956.9

TABLE 2.- POSITION LANDMARKS

Benchmark	Latitude	Longitude	Elevation
Moffett Field			
A	37° 24' 57"	122° 03' 17"	13.31 ft
B	37° 24' 56"	122° 03' 20"	13.80 ft
D	37° 24' 58"	122° 03' 22"	13.45 ft
Crows Landing			
AP	37° 24' 48"	121° 06' 26"	141.05 ft
L	37° 24' 47"	121° 06' 17"	138.53 ft
R	37° 24' 04"	121° 06' 36"	164.71 ft
MTR	37° 25' 06"	121° 06' 11"	129.59 ft
N	37° 25' 30"	121° 06' 17"	127.46 ft
P	37° 25' 22"	121° 06' 19"	129.43 ft
M	37° 24' 55"	121° 06' 16"	134.97 ft
TTR	37° 25' 03"	121° 06' 08"	129.87 ft

TABLE 3.- SUMMARY OF TETRAD UH-1B FLIGHT TESTS EXPERIMENTAL DATA FOR 1977

Flight date, 1977	Mode	Alignment heading, deg	Alignment duration, min	Navigation duration sec	Flight duration, sec	Gyro data recorded, sec	Final north velocity error, ft/sec, knots	Final east velocity error, ft/sec, knots	Final velocity error, knots	Final north position error, n. mi.	Final east position error, n. mi.	Final RSS position error, n. mi.
6/9	Triad	X	10	4320					2.8	-0.2	-0.72	0.75
6/10	Triad	X	2	2760					3.0	.4	.4	.69
7/28	Triad	53.0	4	3121	2980	None	3.00 1.78	1.75 1.04	2.06	.40	.16	.43
7/28	Triad	11.0	6.2	6350	5800	None	-11.75 -6.96	-11.13 -6.59	9.59	-5.0	-1.75	5.30
7/28	Triad	25.5	3.2	3821	3460	None	-2.63 -1.56	.38 .23	1.57	1.90	.32	1.93
8/04	Tetrad	50.9	4	4250	3742	None	-6.38 -3.78	.63 .37	3.80	-1.90	1.59	2.48
9/14	Tetrad	52.2	5.2	5528	4950	None	-3.75 -2.22	-.88 -.52	2.28	2.00	-1.19	2.33
9/14	Tetrad	154.4	---	4908	4100	None	-13. -7.70	1.88 1.11	7.78	-.80	-.87	1.18
11/18	Tetrad	49.7	---	3953	2325	None	.875 .52	12.125 7.18	7.20	1.48	-2.33	2.76
11/22	Tetrad	54.3	---	2866	1283	None	-1.625 -.95	2.875 1.70	1.96	-.20	-.02	.20
11/22	Tetrad	49.9	3	2364	1480	None	-2.00 -1.18	.625 .37	1.24	-.19	.22	.29
11/22	Tetrad	51.2	2	1748	1080	None	1.875 1.11	-.875 -.52	1.23	.40	.16	.43

TABLE 4.- SUMMARY OF REDUCED TETRAD UH-1B FLIGHT TESTS DATA FOR 1977

Flight date, 1977	Apparent navigation error growth, knots	North drift rate, deg/hr	North tilt, deg	East drift rate, deg/hr	East tilt, deg	Gyro parity error, max	Gyro parity error, min	Accelerator parity error, max	Accelerator parity error, min	Geographic area	Altitude barometric stabilization	Radar position
6/9	0.51	-0.0082	0.0066	-0.0017	-0.0035					South Bay	No	No
6/10	.82	-.0054	.0058	.0126	.0019					South Bay	No	No
7/28	.05	.0009	.0010	.0000	.0027					Ames Stockton	Yes	No
7/28	2.28	-.0194	.0177	-.0327	-.0044					Stockton-Crows	Yes	Yes
7/28	.92	.0013	.0022	.0153	.0121					Stockton Moffett	Yes	No
8/04	1.91	.0191	.0007	-.0256	.0090	3.25	-3.60	14.71	-15.29	South Bay	Yes	No
9/14	2.12	-.0125	-.0032	.0331	-.0017	3.38	-3.90	15.25	-15.61	Moffett-Crows	Yes	Yes
9/14	.60	-.0097	.0047	-.0025	.0036	3.68	-3.55	20.66	-18.41	Crows-Moffett	Yes	Yes
11/18	1.81					3.60	-3.55	13.84	-13.66	Moffett area	No	No
11/22	.26					3.65	-3.84	12.95	-12.72	Moffett area	No	No
11/22	.53					3.41	-3.98	11.99	-12.58	Moffett area	No	No
11/22	1.01					3.38	-3.55	12.04	-11.95	Moffett area	No	No

TABLE 5.- SUMMARY OF TETRAD UH-1H FLIGHT TEST EXPERIMENTAL DATA FOR 1978

Flight date	Mode	Alignment heading, deg	Alignment duration, min	Navigation duration, sec	Flight duration, sec	Gyro data recorded, sec	Final north velocity error, ft/sec, knots	Final east velocity error, ft/sec, knots	Final velocity error, knots	Final north position error, n. mi.	Final east position error, n. mi.	Final position error, n. mi.
11/17	Triad (invalid)	-128.5	3.0	7464	5288	None	-29.875 -17.77	-1.1625 -.96	17.79	-14.32	3.47	14.739
11/22	Triad	230.8	3.6	3856	2762	None	-14.250 -8.44	-12.000 -7.11	11.04	-3.00	1.36	3.30
12/7	Triad (invalid)	-130.7	3.0	5945	5085	1140	52.5 31.10	-71.0 -42.07	52.32	-11.56	.48	11.57
12/8	Triad	232.6	3.5	6788	~6450	1415	-14.75 -8.74	1.25 .74	8.77	-5.63	.046	5.63
12/13	Tetrad	51.7	3.0	3420	3046	1141	2.250 1.33	-8.750 -5.18	5.35	-1.28	-5.16	5.32
12/21	Tetrad	-131.3	4.0	6671	6315	1053	-7.375 -4.37	11.125 6.59	7.91	-4.16	-.21	4.17

TABLE 6.- SUMMARY OF REDUCED TETRAD UH-1H FLIGHT-TEST DATA FOR 1978

Flight date	Apparent navigation error, knots	North drift rate, deg/hr	North tilt, deg	East drift rate, deg/hr	East tilt, deg	Gyro parity error, max	Gyro parity error, min	Accelerator parity error, max	Accelerator parity error, min	Available position references	Geographic area
11/17	~7 invalid	[a]	[a]	[a]	[a]	[a]	[a]	[a]	[a]	Radar	To Crows
11/22	2.2	0.0185	-0.0098	-0.0320	0.0080					Way points	South Bay
12/7	6.9 invalid	-.0358	-.0376	-.1101	-.0074					DME radar	South Bay
12/8	2.3	.0005	-.0113	-.0374	-.0077					DME radar	To Crows
12/13	.7	.0075	-.0103	-.0079	.0018					DME radar	To Crows
12/21	2.6	.0157	-.0192	-.0405	.0098					DME radar	To Crows

[a]Data not available.

TABLE 7.- SUMMARY OF TETRAD FLIGHT TEST EXPERIMENTAL DATA FOR 1979

Flight date	Mode	Alignment heading, sec	Alignment duration, min	Navigation duration, sec	Flight duration, sec	Gyro data recorded, sec	Final north velocity error, ft/sec, knots	Final east velocity error, ft/sec, knots	Final velocity error, knots	Final north position error, n. mi.	Final east position error, n. mi.	Final RSS position error, n. mi.	Final RSS position error, knots
5/25/79	Triad	291	6.0	3696	3396	992	6.25 3.70	-7.75 -4.59	5.00	1.26	-0.29	1.29	1.26
5/25/79	Tetrad	292	4.1	3111	2610	974	4.25 2.52	-7.125 -4.22	4.92	-1.56	-.33	1.60	1.85
5/29/79	Tetrad	292	4.0	3078	2898	992	-8.875 -5.26	-10.50 -6.22	8.15	-2.4	1.52	2.84	3.33
6/05/79	Tetrad	289	7.0	3468	3302	992	-6.125 -3.63	-2.625 -1.56	3.95	-4.02	0	4.02	4.17
6/05/79	Tetrad	290	5.0	3286	3112	995	-.875 -.52	-13.25 -7.85	7.87	-2.64	-1.33	2.96	3.24
6/05/79	Triad	288	6.4	3005	2834	992	-5.0 -2.96	-6.875 -4.07	5.04	-3.12	-.67	3.19	3.82
6/05/79	Triad	293	5.0	3083	2939	992	-1.25 -.74	-13.0 -7.70	7.74	-1.44	-1.72	2.24	2.62
6/06/79	Triad	294	6.9	3586	3249	992	4.25 2.52	-6.0 -3.55	4.36	.66	-1.29	1.45	1.45
6/06/70	Triad	293	4.0	3361	3121	994	3.0 1.78	-6.125 -3.63	4.04	-1.56	-.48	1.63	1.75
6/07/79	Tetrad	292	4.2	3262	3106	992	-2.25 -1.33	-8.0 -4.74	4.92	-1.32	-1.10	1.72	1.89
6/07/79	Tetrad	292	4.0	3080	3213	992	-1.5 -.030	-7.375 -4.67	4.46	-2.16	-1.05	2.40	2.81

TABLE 8.- SUMMARY OF REDUCED TETRAD FLIGHT TEST DATA FOR 1979

Flight date	Apparent navigation error, knots	North drift rate, deg/hr	North tilt, deg	East drift rate, deg/hr	East tilt, deg	Gyro parity error, max	Gyro parity error, min	Accelerator parity error, max	Accelerator parity error, min
5/25/79	1.97	-0.0002	-0.0075	0.0328	-0.0095	---	---	---	---
5/25/79	1.80	.0288	-.0145	-.0082	-.0099	---	---	---	---
5/29/79	4.01	.0415	-.0096	-.0523	.0057	---	---	---	---
6/05/79	4.04	.0088	-.0061	-.0668	.0037	3.6	-3.7	1.13	-1.22
6/05/79	3.76	.0281	-.0099	-.0561	-.0038	3.4	-3.8	1.17	-1.30
6/05/79	3.35	.0189	-.0066	-.0526	.002	3.3	-3.3	1.26	-1.28
6/05/79	3.63	.0530	-.0134	-.0292	.000	3.7	-3.7	1.44	-1.29
6/06/79	1.37	.0131	-.0019	-.0187	-.0003	3.1	-3.5	1.16	-1.30
6/06/79	1.23	.0101	-.0057	-.0178	-.0045	3.7	-3.6	1.35	-1.26
6/07/79	2.08	.0278	-.0070	-.0208	-.0010	---	---	---	---
6/07/70	2.59	.0341	-.0101	-.0264	-.0050	3.9	-3.7	1.14	-1.51

TABLE 9.- SUMMARY OF TETRAD FLIGHT TEST EXPERIMENTAL DATA FOR 1980

Flight date	Mode	Alignment heading, sec	Alignment duration, min	Navigation duration, sec	Flight duration, sec	Gyro data recorded, sec	Final north velocity error, ft/sec, knots	Final east velocity error, ft/sec, knots	Final velocity error, knots	Final north position error, n. mi.	Final east position error, n. mi.	Final RSS position error, n. mi.
4/01/80	Triad	50	5.0	5878	3614	992	-3.0 -1.78	3.875 2.30	2.90	-2.04	0.81	2.23
4/01/80	Triad	140	5.0	5620	5004	991	-4.5 -2.67	7.250 4.30	5.06	-2.34	.81	2.48
4/07/80	Triad	217	5.0	5874	4851	991	-3.375 -2.00	2.5 1.48	2.49	-1.86	.91	2.07
4/15/80	Triad	230	5.0	5678	4371	993	-9.375 -5.55	1.125 .67	5.59	-4.98	.24	4.99
4/17/80	Triad	52	5.0	6677	5564	992	6.875 4.07	-7.250 -4.30	5.92	-1.74	1.86	2.55
5/15/80	Triad malfunction	233	5.0	5457	4692	1112	-47.750 -28.29	46.875 27.77	39.65	-28.08	-9.20	29.55
5/21/80	Tetrad diagnostic	233	5.0	6248	5780	1111	-12.125 -7.18	3.125 1.85	7.42	-3.84	-.29	3.85
5/22/80	Triad	48	5.0	5342	4306	992	-7.875 -4.67	15.875 9.41	10.50	-4.14	.29	4.15
5/29/80	Tetrad diagnostic using only triad sensors	229	5.0	5241	4838	0	2229.375 1320.88	-3875.750 -2296.33	2649.12	-42.18	78.37	88.97
6/02/80	Triad	228	5.0	6198	4655 672	0	-8.000 -4.74	3.125 1.85	5.09	-2.58	1.05	2.78

TABLE 10.- SUMMARY OF REDUCED TETRAD FLIGHT TEST DATA FOR 1980

Flight date	Apparent navigation error, knots	North drift rate, deg/hr	North tilt, deg	East drift rate, deg/hr	East tilt, deg	Gyro parity error, max	Gyro parity error, min	Accelerator parity error, max	Accelerator parity error, min
4/01/80	<1.5								
4/01/80	<1.5								
4/07/80	1.34	-0.0122	-0.0067	-0.0187	0.0028				
4/15/80	2.26	-.0013	-.0065	-.0376	.0052				
4/17/80	1.06	-.0057	-.0106	-.0167	.0041				
5/15/80	>15.	Not estimated				7.66	-6.25	-1.49	-1.47
5/21/80	~1.5	Before velocity jump at 600 sec				8.61	-5.66	1.53	-1.39
5/22/80	3.5	Not recorded							
5/29/80	Large	Not estimated				422.86	-388.30	1.49	-1.62
6/02/80	1.8	Not recorded							

TABLE 11.- FINAL POSITION ERRORS

Year	Mean final position error, n. mi.		Standard deviation of final position error, n. mi.	
	Triad	Tetrad	Triad	Tetrad
1977	1.81	1.38	2.03	1.12
1978	4.5	5.04	1.6	.77
1979	2.2	2.6	1.1	.72
1980	3.13		1.1	
Total[a]	2.66		1.48	

[a]Four-year total, combined triad and tetrad.

TABLE 12.- FINAL VELOCITY ERRORS

Year	Mean final velocity error, knots		Standard deviation of final velocity error, knots	
	Triad	Tetrad	Triad	Tetrad
1977	3.84	3.6	2.93	2.8
1978	9.9	6.68	1.8	1.63
1979	5.42	5.7	1.5	1.8
1980	5.4		2.6	
Total[a]	5.06		3.84	

[a]Four-year total, combined triad and tetrad.

TABLE 13.- TEST RESULTS OF STATIC LABORATORY TESTS OF TETRAD INS

Run	Date, 1977	Heading	Mode	Alignment, min	Navigation, min	Final velocity error, knots
1	12/7	N	Tetrad	10	41	0.8
2					44	1.9
3					30	1.3
4					30	1.4
5					30	2.0
6			Triad		30	1.6
7			Triad		34	1.0
1	12/8	N	Triad	10	30	0.7
2			Triad	10	31	1.8
3			Tetrad	5	45	1.6
4				4	48	3.1
5				3	24	2.8
6				2	47	2.9
7				1	254	2.7
1	12/9	E	Tetrad	10	38	2.4
2					34	2.6
3					49	1.7
4					37	2.1
5					22	1.0
6			Triad		31	2.1
7			Triad		45	2.5
1	12/10	E	Triad	10	31	1.3
2			Triad	10	35	2.2
3			Tetrad	5	46	1.9
4				4	46	1.1
5				3	50	.8
6				2	46	3.2
7				1	53	.6
1	12/12	S	Tetrad	10	39	1.5
2					35	.7
3					42	1.0
4					34	.3
5					35	.7
6			Triad		39	2.3
7			Triad		196	.7

TABLE 14.- SUMMARY OF TETRAD NONFLIGHT NAVIGATION TESTS: TRIAD MODE

Test data	Apparent navigation errors		Conditions	Alignment time, sec	Navigation time, sec	North drift rate, deg/hr	East drift rate, deg/hr	rms north, ft/sec	rms east, ft/sec
	Position, n. mi.	Velocity, knots							
1979									
5/16/79	0.56		X-Axis pointing south	503	1068	0.0088	-0.0033	0.0762	0.0413
5/16/79	1.14		X-Axis pointing east	643	2522	.0188	-.0026	.0848	.0922
1980									
1/18/80	0.44	0.45	Z-Axis pointing south	538	7217	0.0061	-0.0041	0.5951	1.0543
3/13/80	.72	1.76	Z-Axis pointing north	368	5673	-.0113	-.0043	.3981	.7135
4/22/80	1.23	.67	Heading change during alignment	301	5430	-.0082	-.0188	.7025	.3010
4/22/80	1.00	.8	Z-Axis pointing north	273	5957	-.0114	-.0122	.2789	.6630
5/06/80	1.18	.89	Z-Axis pointing west 10-40-Hz motion	301	5070	.0182	-.0074	.6139	.2208
5/07/80	1.36	.6	Z-Axis pointing west 10-40-Hz motion	301	5575	.0132	-.0184	.6451	.7213
Summary of 1979, 1980 tests									
Mean position error 0.95 n. mi. Standard deviation 0.34 n. mi.					Mean velocity error 0.86 knots Standard deviation 0.47 knots				

TABLE 15.- ORTHOGONAL-GYRO DETECTION INVERVALS VERSUS STEP FAILURE FOR STATIONARY, 0.1-Hz, 2-Hz, AND FLIGHT-TEST MOTION ENVIRONMENTS

Simulated step bias error, deg/hr	Detection time intervals in data frames [a]											
	Stationary			0.1 Hz			2 Hz			Flight data, ~10.5 Hz		
	1[b]	2[c]	3[d]	1[b]	2[c]	3[d]	1[b]	2[c]	3[d]	1[b]	2[c]	3[d]
10	0	0	0	0	0	0	0	0	0	5	5	5
20	0	0	0	0	0	0	0	0	0	5	5	5
30	0	0	0	0	0	0	0	0	0	5	5	5
40	0	0	0	0	0	0	0	0	1	5	5	4
50	0	0	0	0	0	0	0	0	2	5	5	4
[1][e] 60	0	0	0	0	0	0	0	1	4	5	4	4
70	0	0	0	0	0	0	0	2	5	5	5	4
80	0	0	0	0	0	0	0	2	6	5	4	4
90	0	0	0	0	0	1	0	4	7	5	4	4
100	0	0	0	0	0	2	0	5	8	5	4	4
110	0	0	0	0	0	3	0	5	11	5	4	6
[2][e] 120	0	0	3	0	0	4	1	6	12	4	4	6
130	0	0	3	0	1	5	1	8	12	4	4	9
140	0	0	13	0	1	9	2	9	15	5	4	15
150	0	0	13	0	2	19	2	10	16	4	4	20
160	0	0	21	0	3	22	2	13	17	4	5	21
170	0	0	21	0	3	28	4	11	23	4	6	26
180	0	3	35	0	4	37	4	13	23	4	6	32
[3][e] 190	0	3	35	0	5	44	4	14	29	4	8	31
200	0	5	52	0	5	50	5	16	26	4	10	32
210	0	13	46	0	9	53	5	19	25	4	15	31
220	0	13	57	0	15	49	5	19	27	4	19	34
230	0	21	50	0	23	45	5	23	31	4	20	38
240	0	21	57	0	24	45	6	25	29	4	22	42
[4][e] 250	0	21	57	0	29	47	6	29	27	4	26	42
260	0	37	43	1	34	43	8	31	27	4	29	40
270	0	38	42	1	40	39	9	31	28	4	34	38
280	0	38	42	1	46	33	9	34	26	4	35	39
290	0	38	42	2	49	29	10	38	23	4	35	39
300	0	57	23	2	53	25	10	36	27	4	38	36
310	0	57	23	2	56	22	12	37	27	5	40	33
[5][e] 320	0	57	23	3	60	17	13	38	26	5	47	26
330	0	70	10	3	62	15	13	39	26	6	49	24
340	0	70	10	3	65	12	13	44	22	6	54	19
350	3	70	7	3	66	11	15	46	18	6	60	13
360	3	75	2	4	66	10	16	45	19	6	62	11
370	3	75	2	5	68	7	16	47	17	7	65	7
[6][e] 380	3	77	0	5	71	4	17	47	16	8	64	7
390	3	77	0	5	73	2	18	49	13	10	63	6
400	5	75	0	6	73	1	19	49	12	10	65	4
[9][e] 500	13	67	0	14	66	0	19	61	0	16	64	0
[11][e] 600	64	16	0	66	14	0	59	21	0	48	32	0
[12][e] 770	80	0	0	80	0	0	80	0	0	80	0	0

[a] Detection threshold is 5 counts.

[b] Cases out of 80 detected in first frame.

[c] Cases out of 80 detected in second frame.

[d] Cases out of 80 detected in third frame.

[e] Approximate counts at indicated degrees per hour step error level.

TABLE 16.- SKEW GYRO DETECTION INTERVAL VS STEP FAILURE FOR STATIONARY, 0.1 Hz, 2 Hz, AND FLIGHT TEST MOTION ENVIRONMENTS

Simulated step bias error, deg/hr	Detection time intervals in detection frames[a]											
	Stationary			0.1 Hz			2 Hz			Flight data, ~10.5 Hz		
	1[b]	2[c]	3[d]	1[b]	2[c]	3[d]	1[b]	2[c]	3[d]	1[b]	2[c]	3[d]
10	0	0	0	0	0	0	0	0	1	5	5	5
20	0	0	0	0	0	0	0	1	1	5	5	4
30	0	0	0	0	0	0	0	1	2	5	4	4
40	0	0	0	0	0	0	0	2	4	5	4	4
50	0	0	0	0	0	0	0	3	8	4	4	4
[1][e] 60	0	0	0	0	0	1	0	4	9	4	4	7
70	0	0	2	0	0	7	1	7	12	4	4	10
80	0	0	10	0	0	12	1	9	13	4	6	17
90	0	0	23	0	0	18	1	11	20	4	7	27
100	0	0	23	0	4	24	2	14	18	3	10	34
110	0	2	41	0	9	32	2	16	23	4	12	33
[2][e] 120	0	10	49	0	11	43	3	17	31	4	17	41
130	0	10	57	0	16	33	7	23	28	4	23	36
140	0	23	43	0	21	54	7	25	31	4	35	36
150	0	23	57	0	27	50	9	24	34	4	42	31
160	0	42	38	0	36	43	9	29	33	6	41	31
170	0	59	21	0	45	35	9	32	35	9	48	24
180	0	59	21	1	53	26	11	39	26	7	53	10
[3][e] 190	0	67	13	2	58	20	12	45	22	10	52	17
200	0	67	13	3	69	8	15	43	22	10	58	12
210	2	73	3	5	70	5	16	47	17	10	63	7
220	2	75	3	8	69	3	17	48	15	13	63	4
230	7	73	0	9	68	3	18	50	12	15	62	3
240	10	70	0	10	69	1	19	52	9	18	60	2
[4][e] 250	10	70	0	11	69	0	23	51	6	22	56	2
260	10	70	0	15	65	0	27	48	5	27	50	3
270	22	58	0	16	64	0	28	48	4	31	46	3
280	22	58	0	20	60	0	30	48	2	37	40	3
290	22	58	0	24	56	0	31	49	0	40	39	1
300	22	58	0	26	54	0	31	49	0	44	35	1
310	41	39	0	30	50	0	32	48	0	44	35	1
[5][e] 320	41	39	0	35	45	0	37	43	0	44	35	1
330	42	38	0	40	40	0	40	40	0	45	34	1
340	58	22	0	44	36	0	41	39	0	51	28	1
350	58	22	0	50	30	0	45	35	0	55	25	0
360	58	22	0	53	27	0	50	30	0	60	20	0
370	58	22	0	56	24	0	54	26	0	61	19	0
[6][e] 380	66	14	0	59	21	0	57	23	0	62	18	0
390	66	14	0	68	12	0	58	22	0	63	17	0
400	66	14	0	71	9	0	58	22	0	68	12	0
420	73	7	0	74	6	0	68	12	0	73	7	0
[7][e] 430	80	0	0	80	0	0	80	0	0	80	0	0

[a]Detection threshold is 5 counts.

[b]Cases out of 80 detected in first frame.

[c]Cases out of 80 detected in second frame.

[d]Cases out of 80 detected in third frame.

[e]Approximate counts at indicated degrees per hour step error level.

TABLE 17.- SAMPLE STATIC INCREMENTAL VELOCITIES FOR IDENTICAL 360° ROTATIONS ABOUT THE PITCH AXIS

Trial[a]	ΔV_x, ft/sec	ΔV_y, ft/sec	ΔV_z, ft/sec
1	0.015	-0.135	-0.274
2	-.013	-.090	-.214
3	-.015	-.096	-.206
4	-.068	-.087	-.183
5	-.044	-.077	-.173

[a]Following alignment, a 360° rotation around the pitch axis was made, followed by a short static navigation.

TABLE 18.- LASER GYRO BIAS COMPENSATIONS

Axis	Bias compensation, deg/hr	% change
1977 laser gyro		
x	+0.16198	---
y	-.0615	---
z	+.0556	---
Skew	+.0195	---
1978-1980 laser gyro		
x	-0.003	98
y	-.0844	37
z	+.1024	84
Skew	+.0195	0

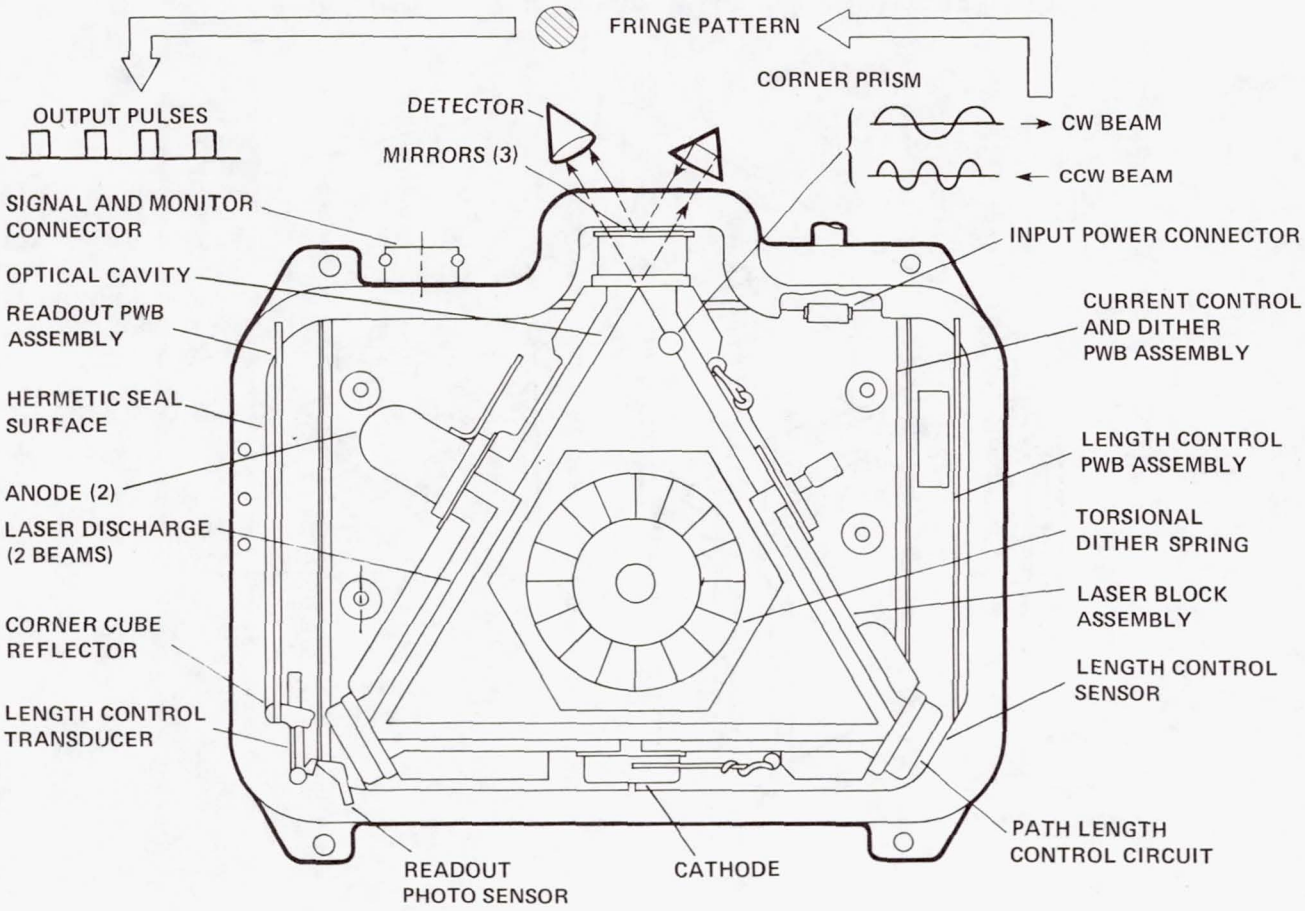

Figure 1.- Basic laser gyro.

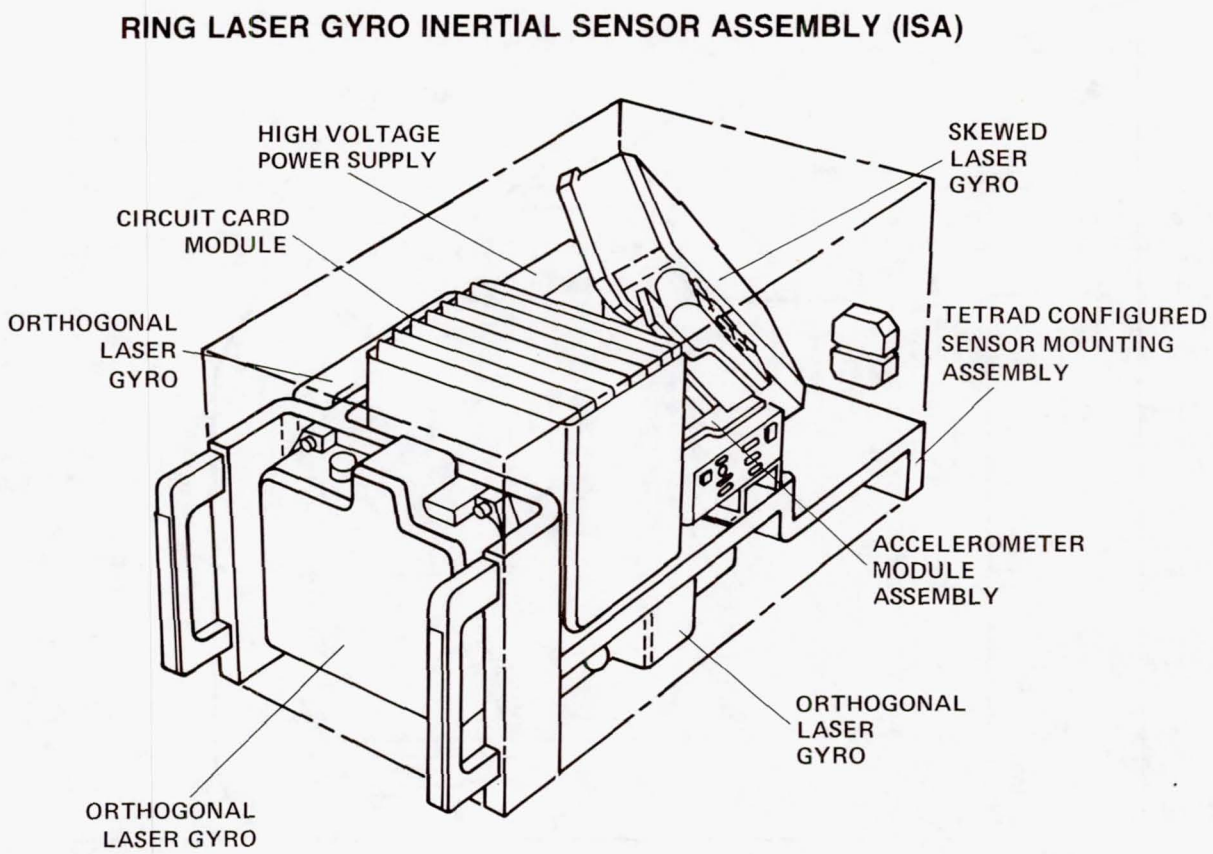

Figure 2.- Inertial sensor assembly.

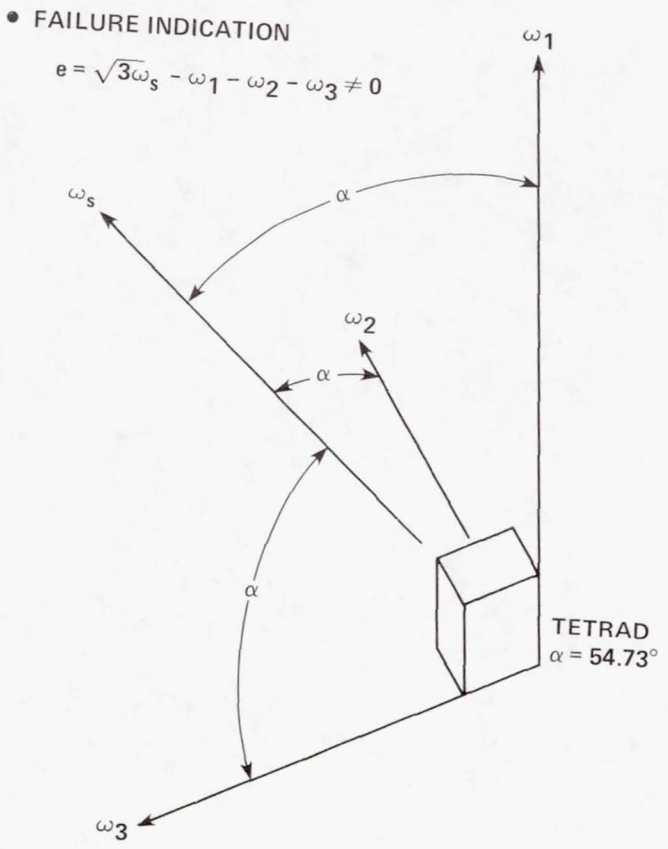

Figure 3.- Sensing-axis geometry of Tetrad.

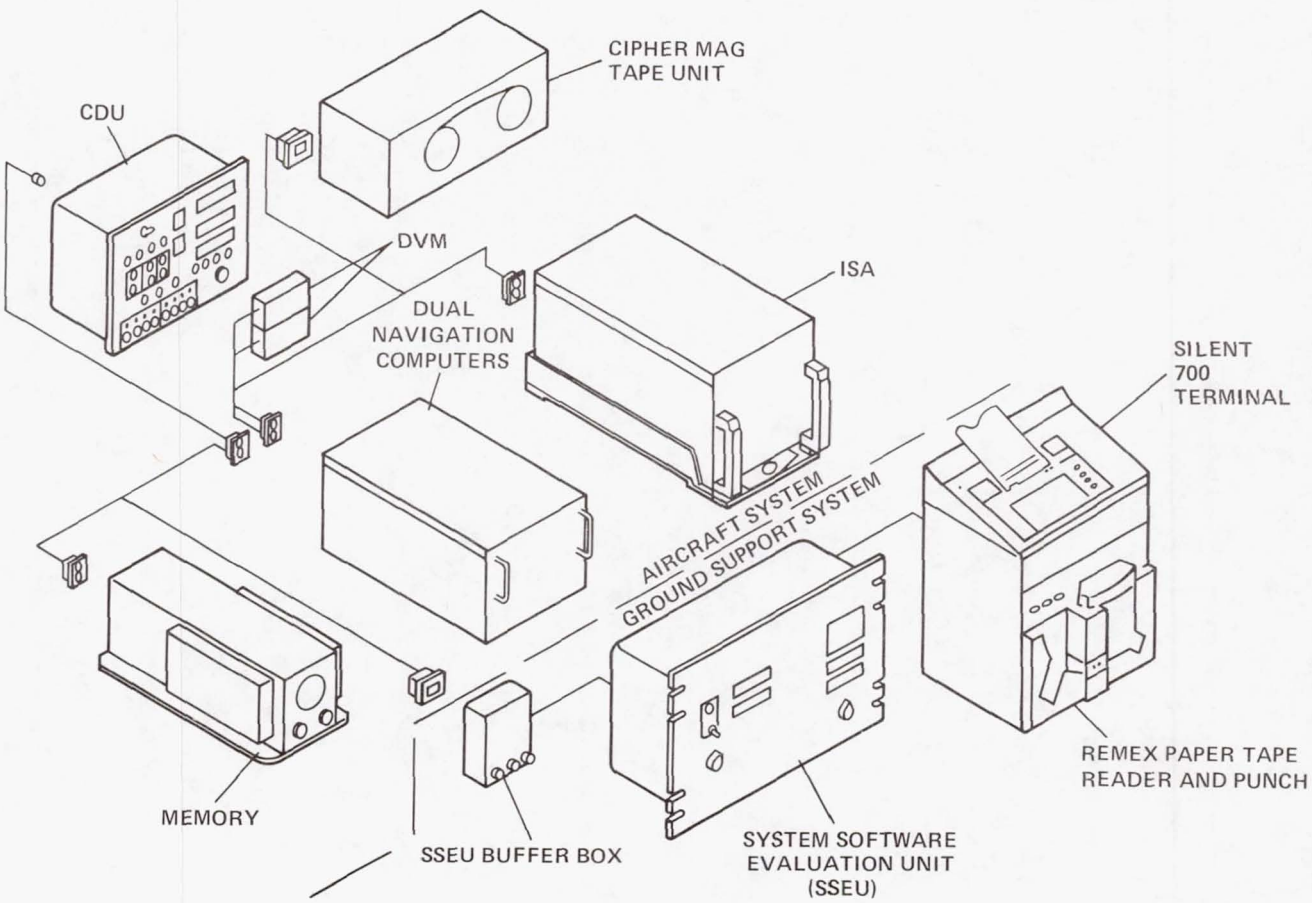

Figure 4.- Tetrad flight system components.

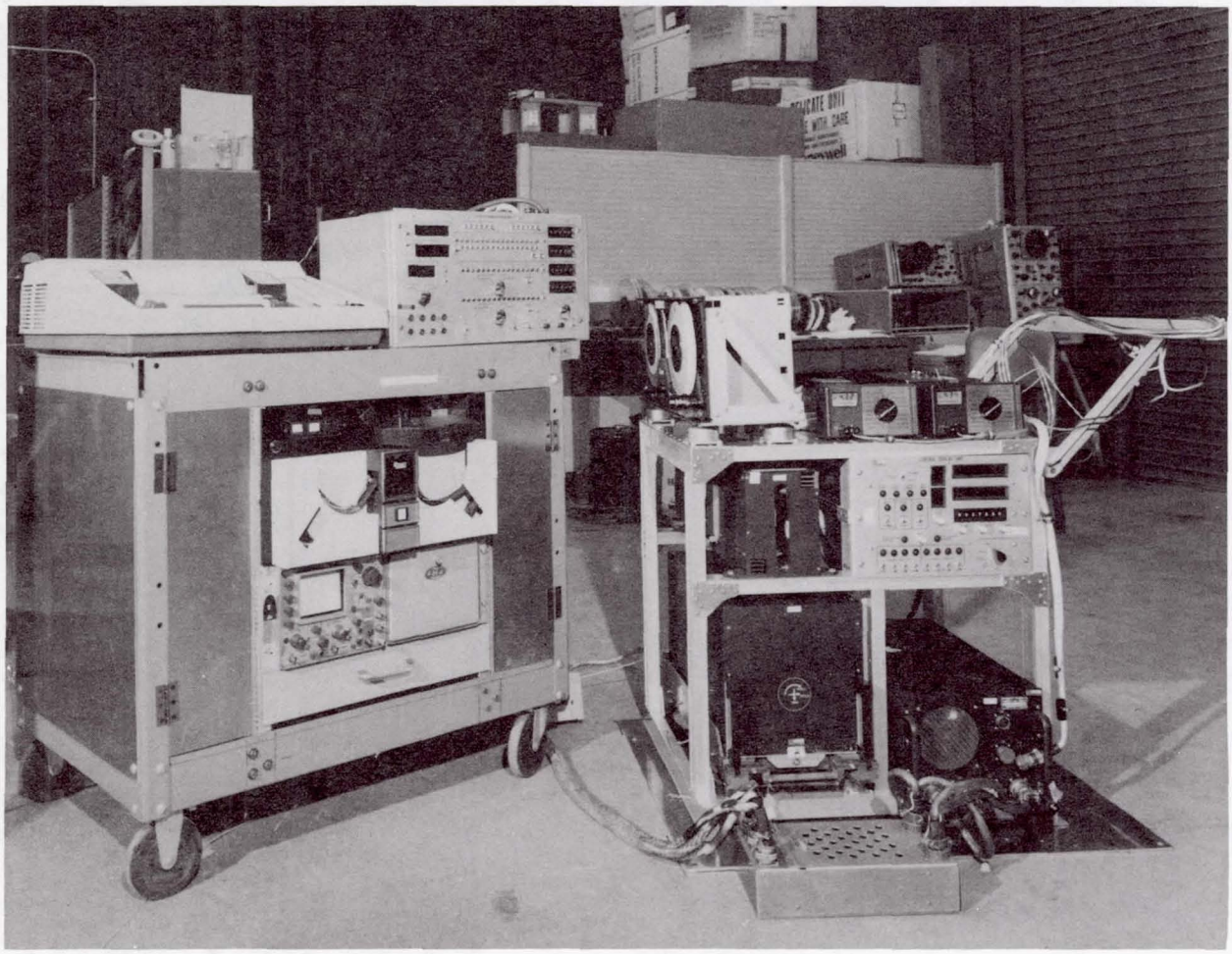

Figure 5.- Tetrad flight- and ground-support system.

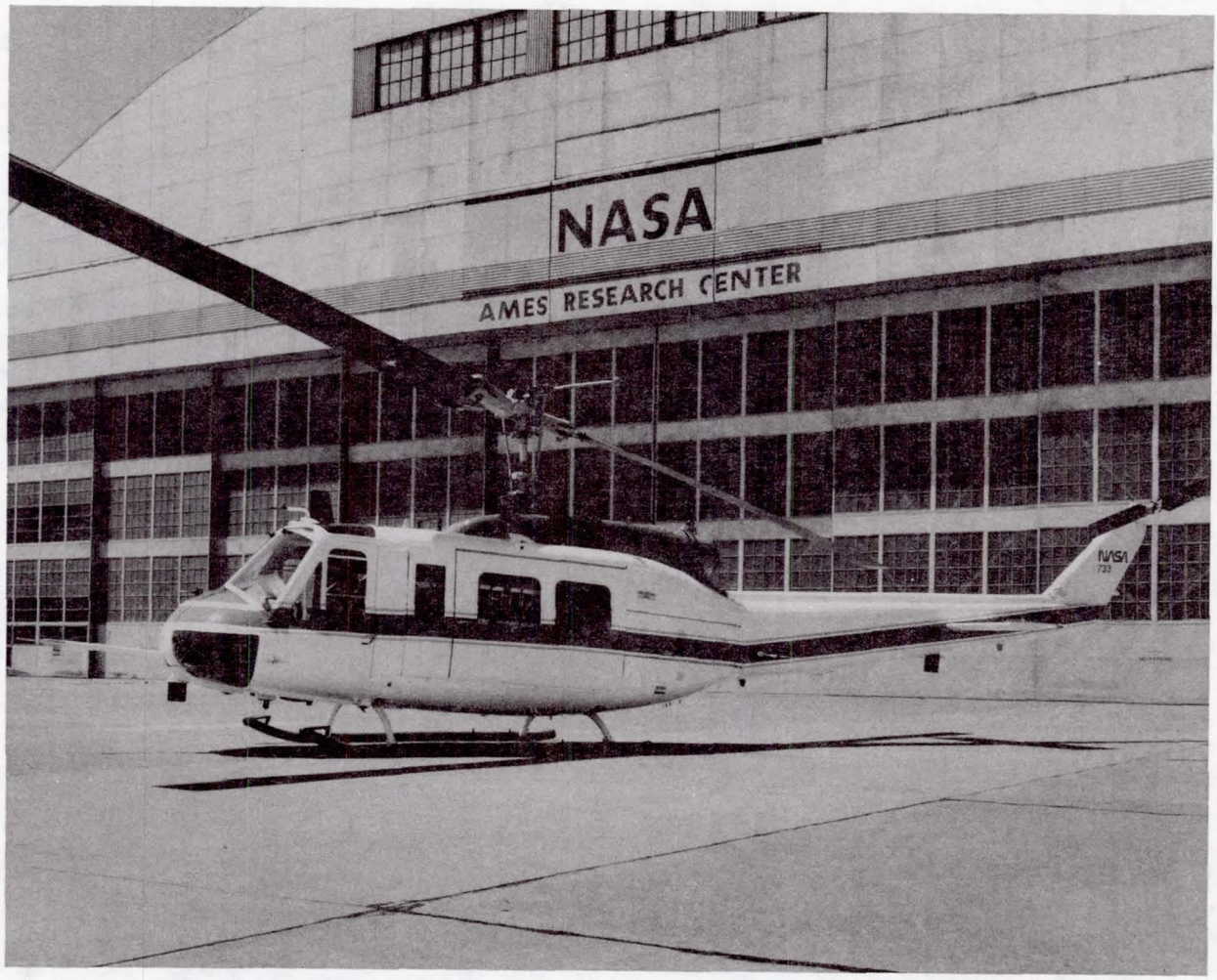

Figure 6.- UH-1H research helicopter.

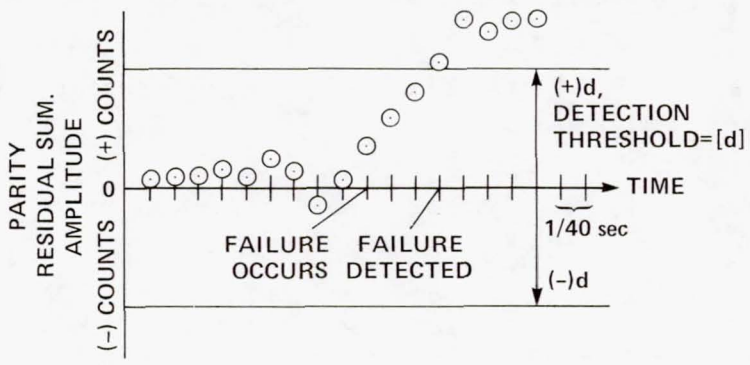

Figure 7.- Parity residual amplitude versus time (in data frames).

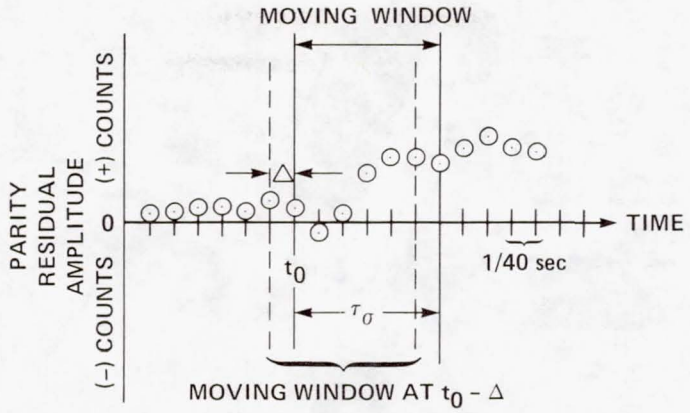

Figure 8.- Parity residual sum versus time (in data frames).

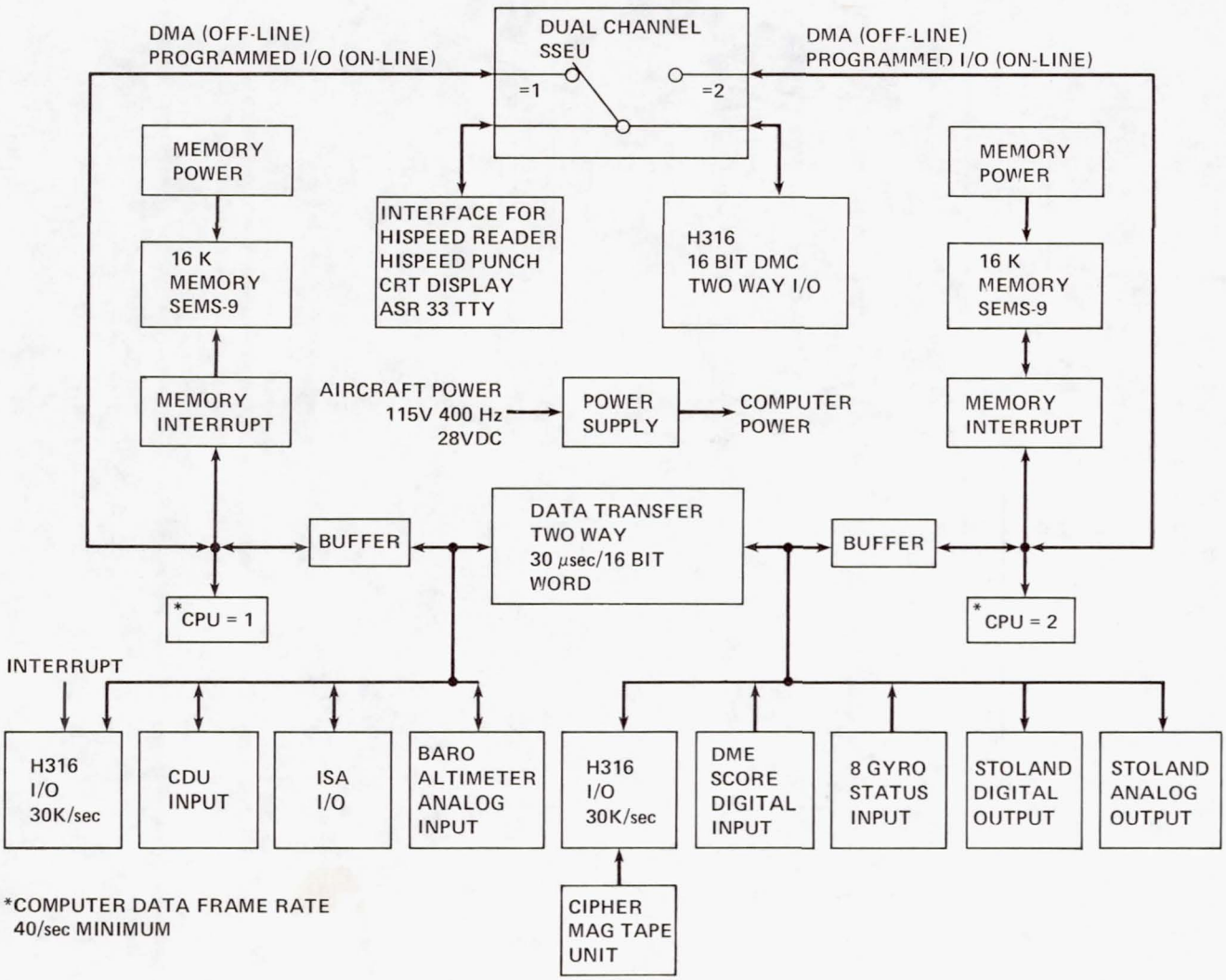

Figure 9.- Tetrad INS computer with system software evaluation unit (SSEU).

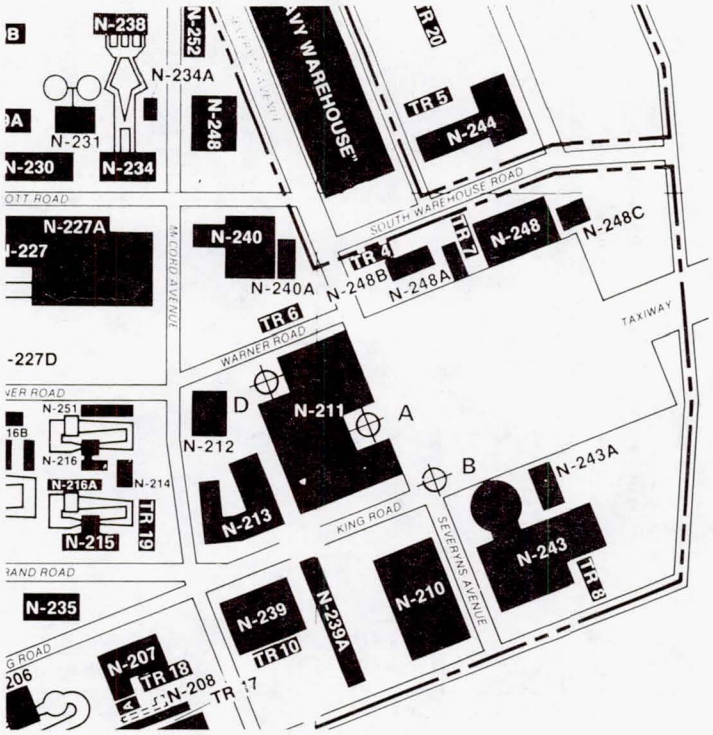

Figure 10.- Landmarks at Moffett Field.

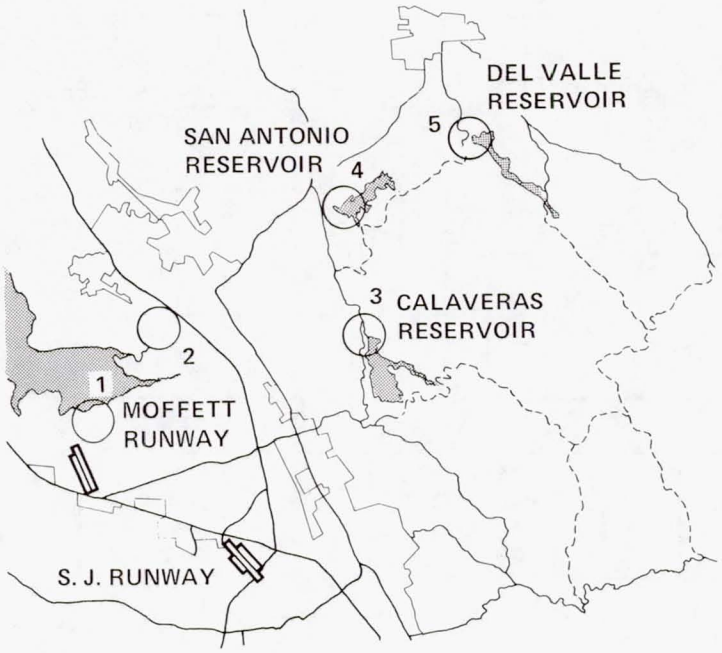

Figure 11.- Flight-test area and visual-navigation landmarks.

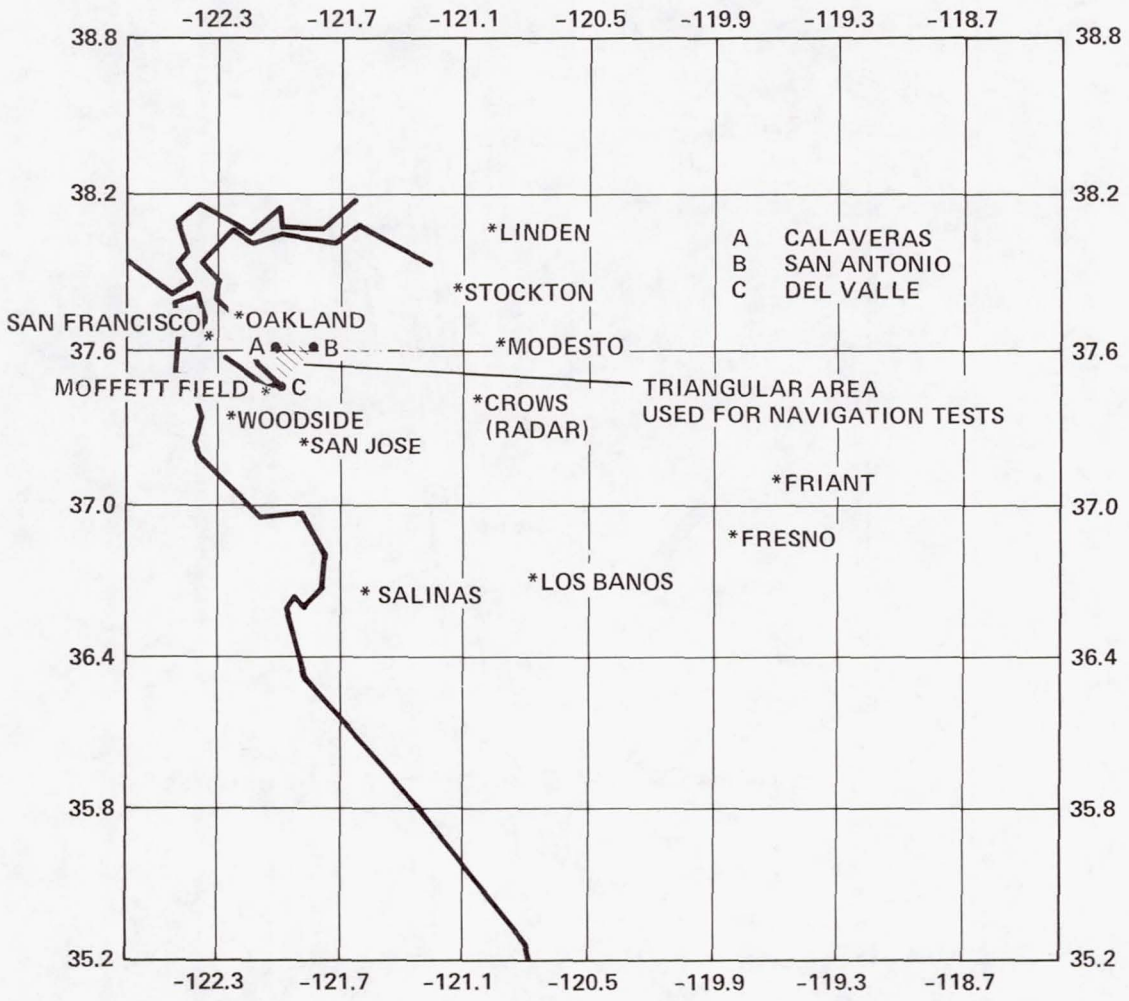

Figure 12.- Position reference locations for DME transponders.

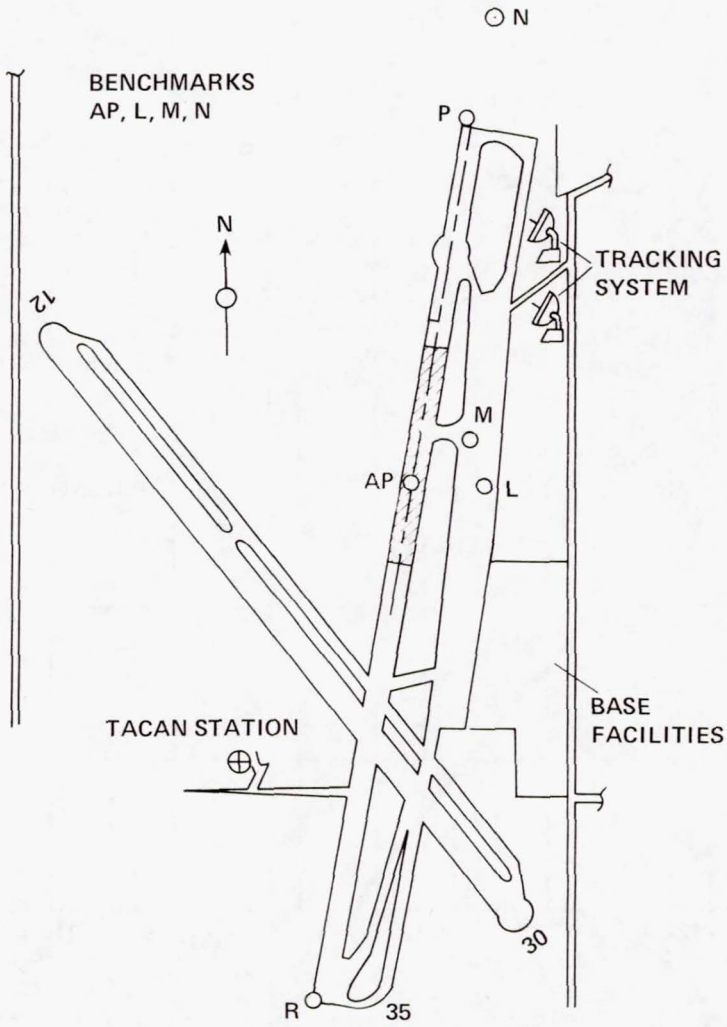

Figure 13.- Landmarks at Crows Landing.

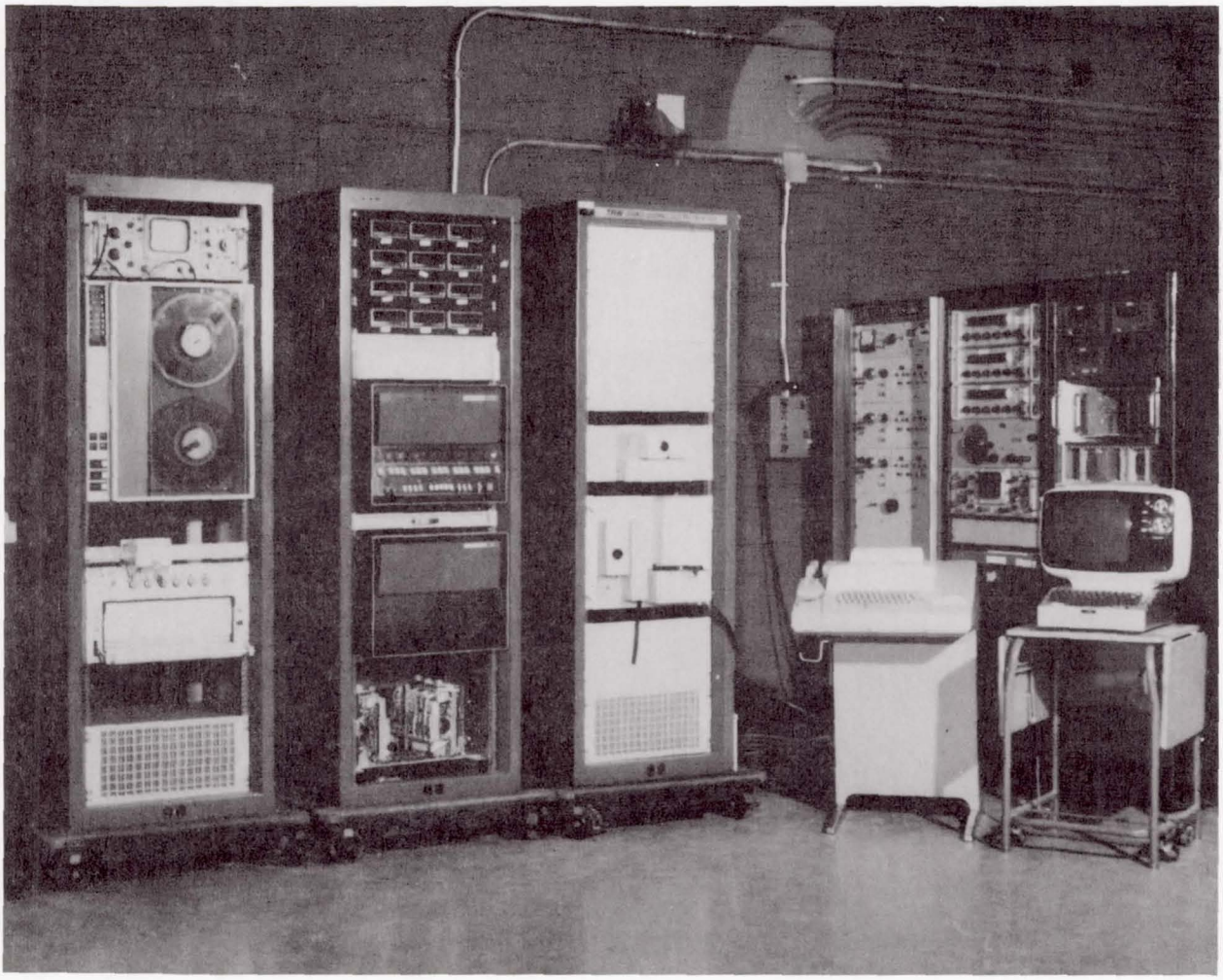

Figure 14.- Motion simulator data acquisition system: minicomputer.

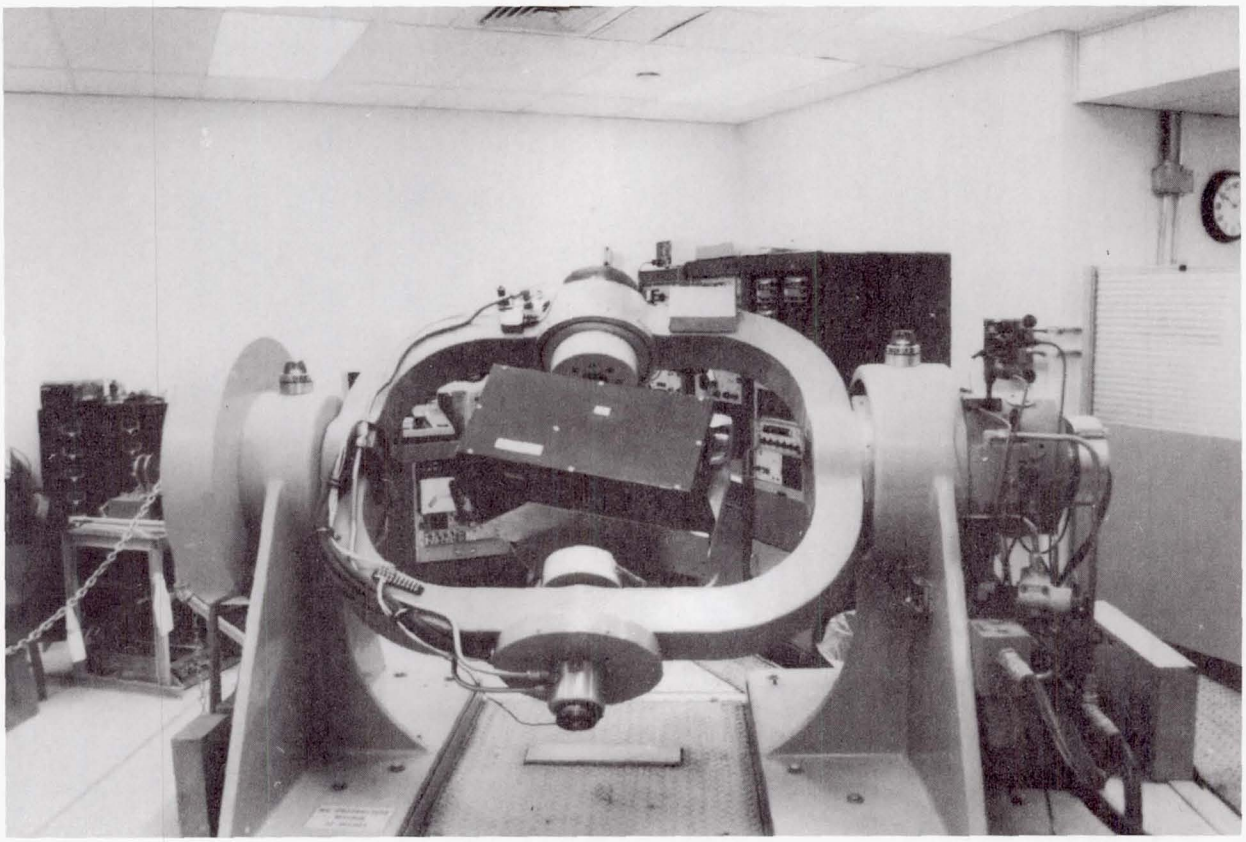

Figure 15.- Inertial sensor assembly mounted on the motion simulator.

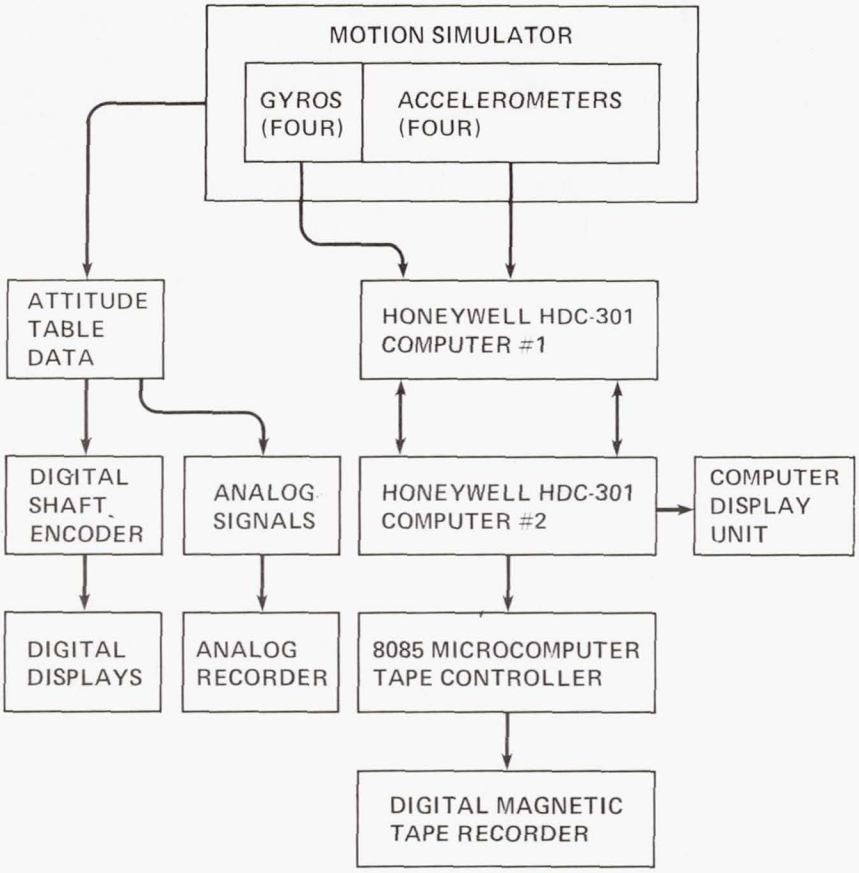

Figure 16.- Data Acquisition system.

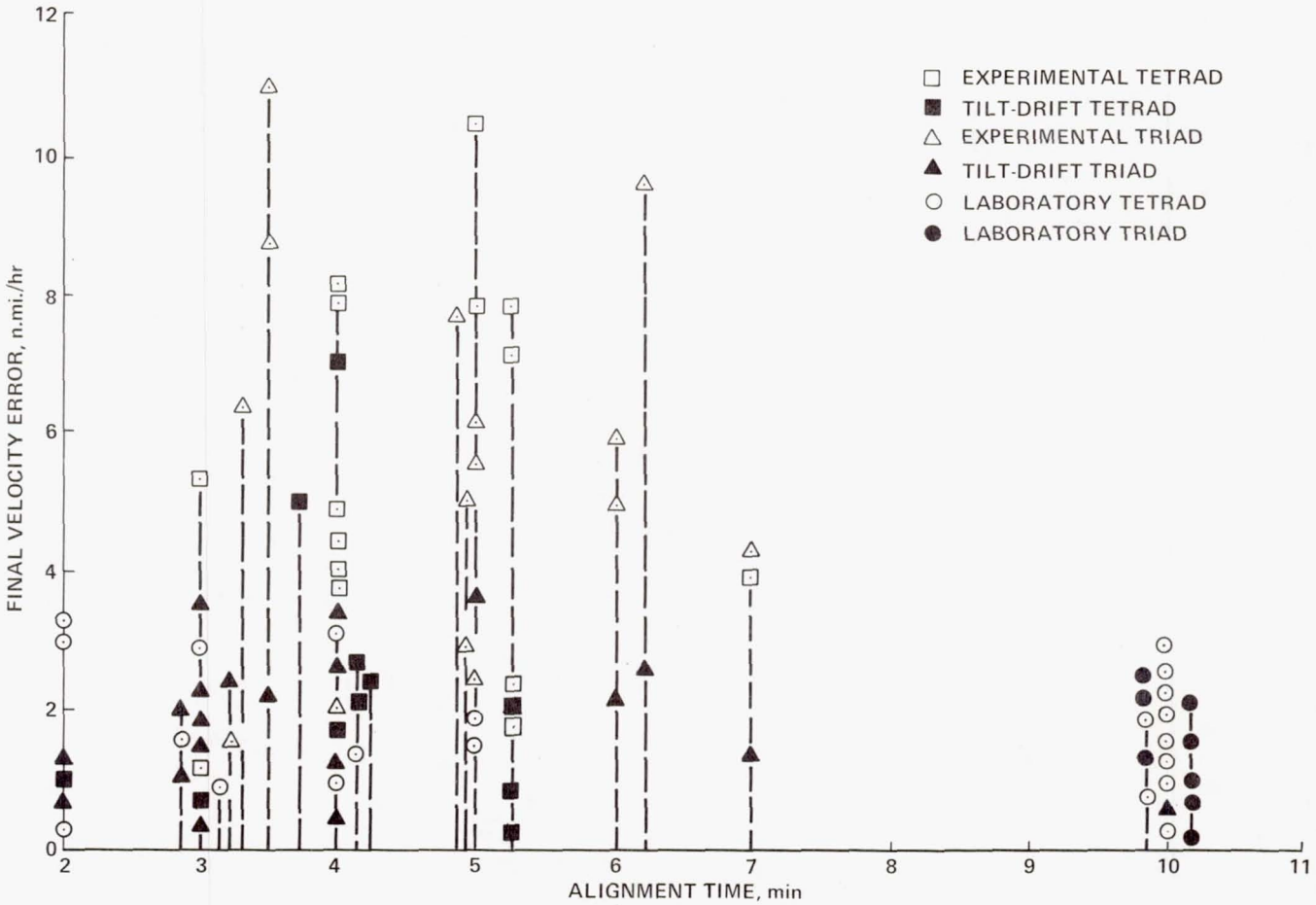

Figure 17.- Final velocity error versus alignment time.

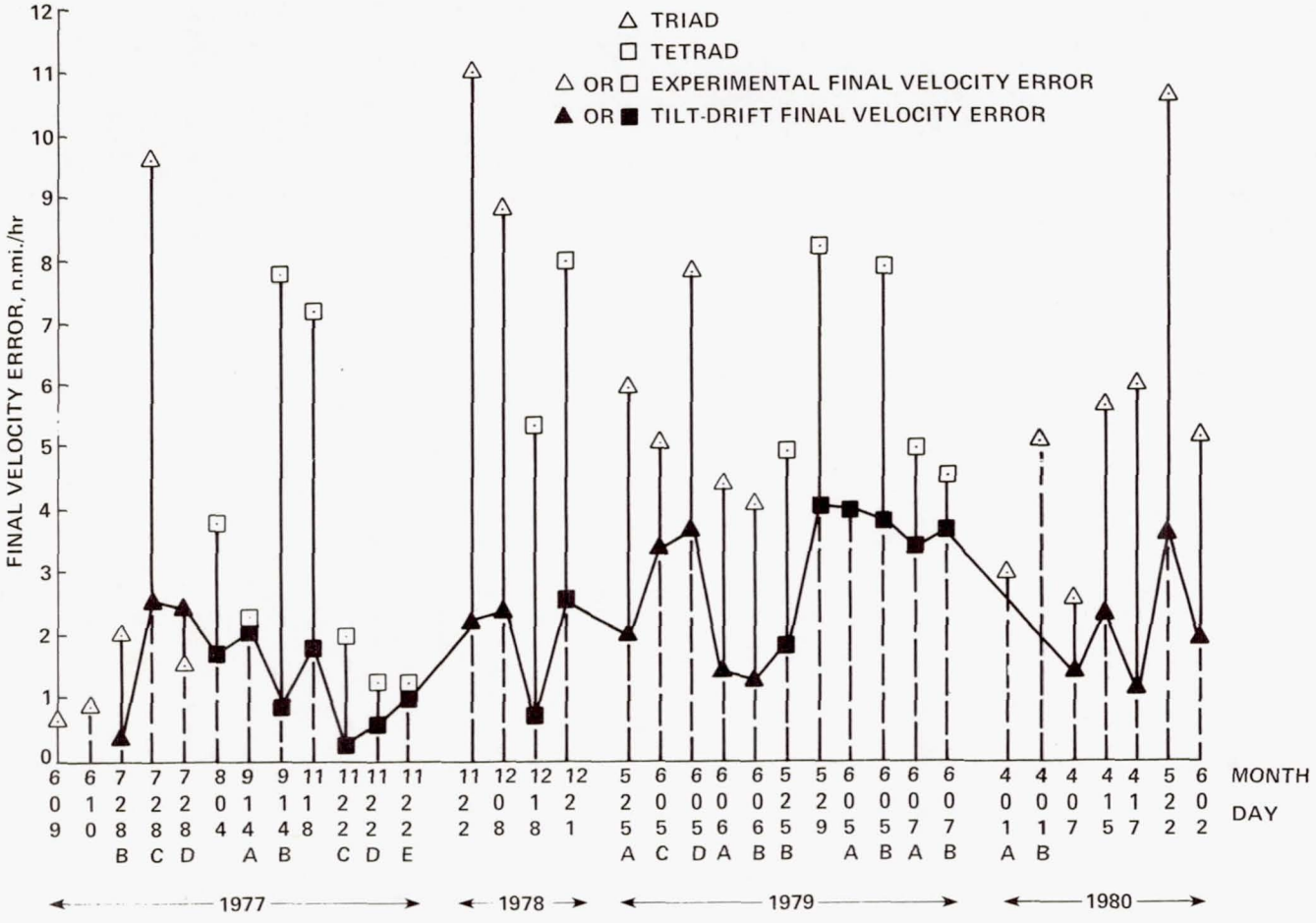

Figure 18.- Summary of final velocity errors: 4 yr of flight test.

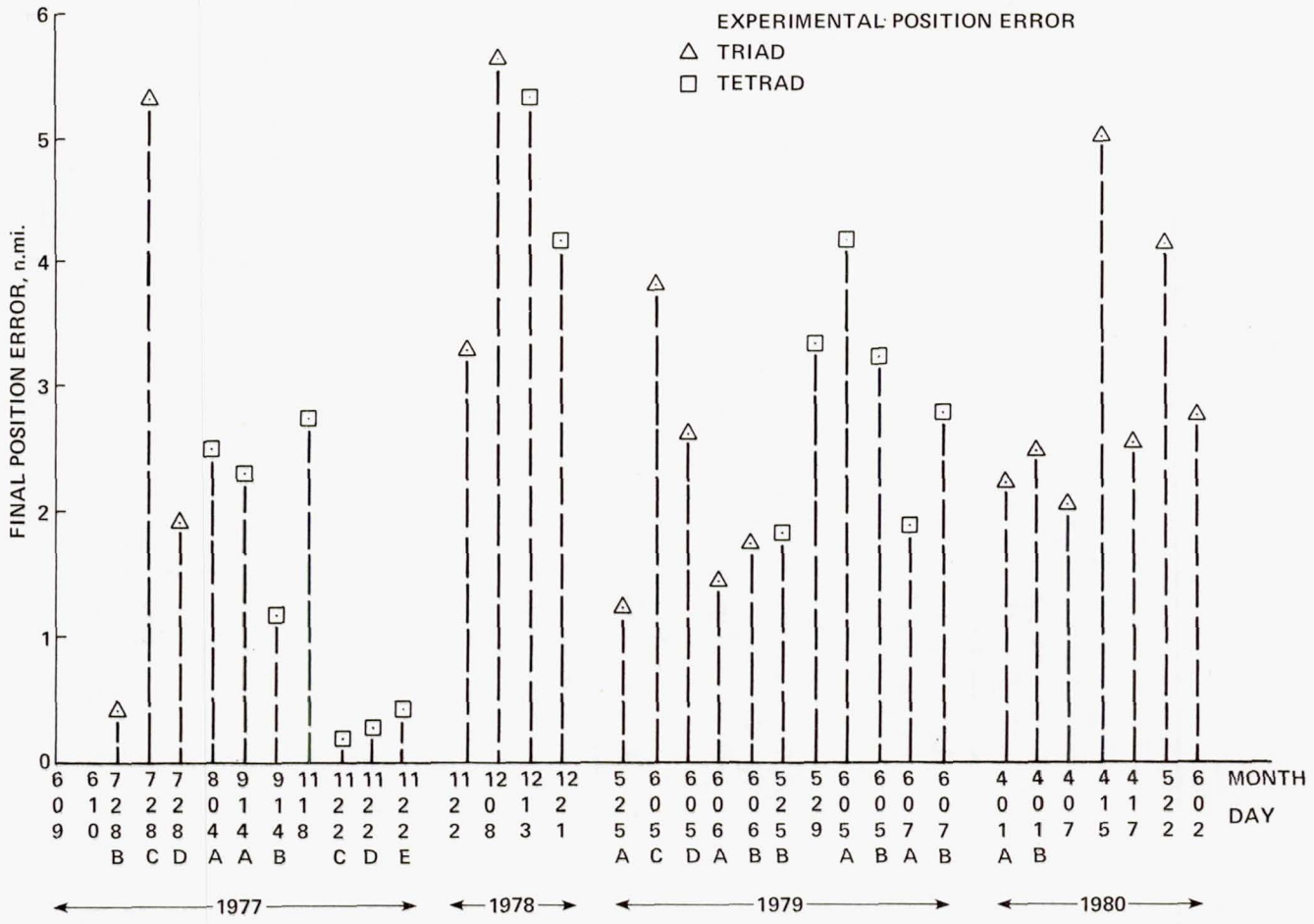

Figure 19.- Summary of final position errors: 4 yr of flight test.

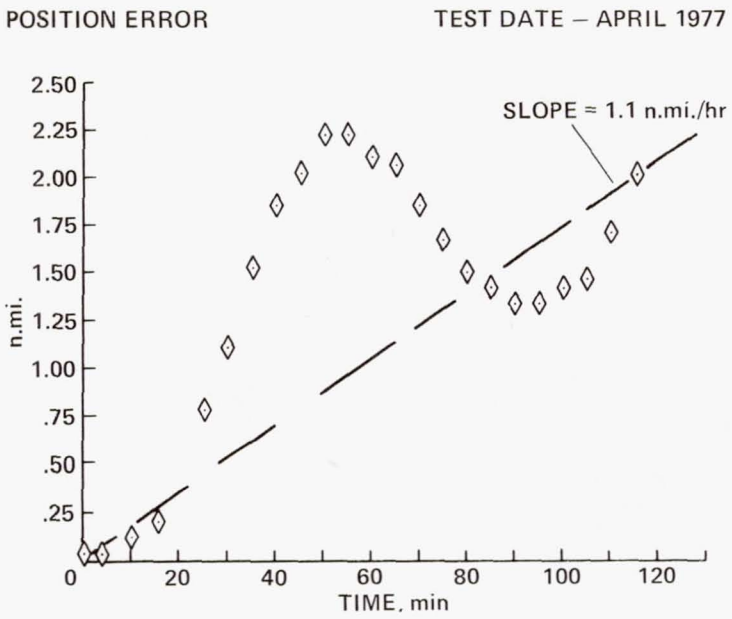

Figure 20.- Position errors: initial static navigation acceptance tests.

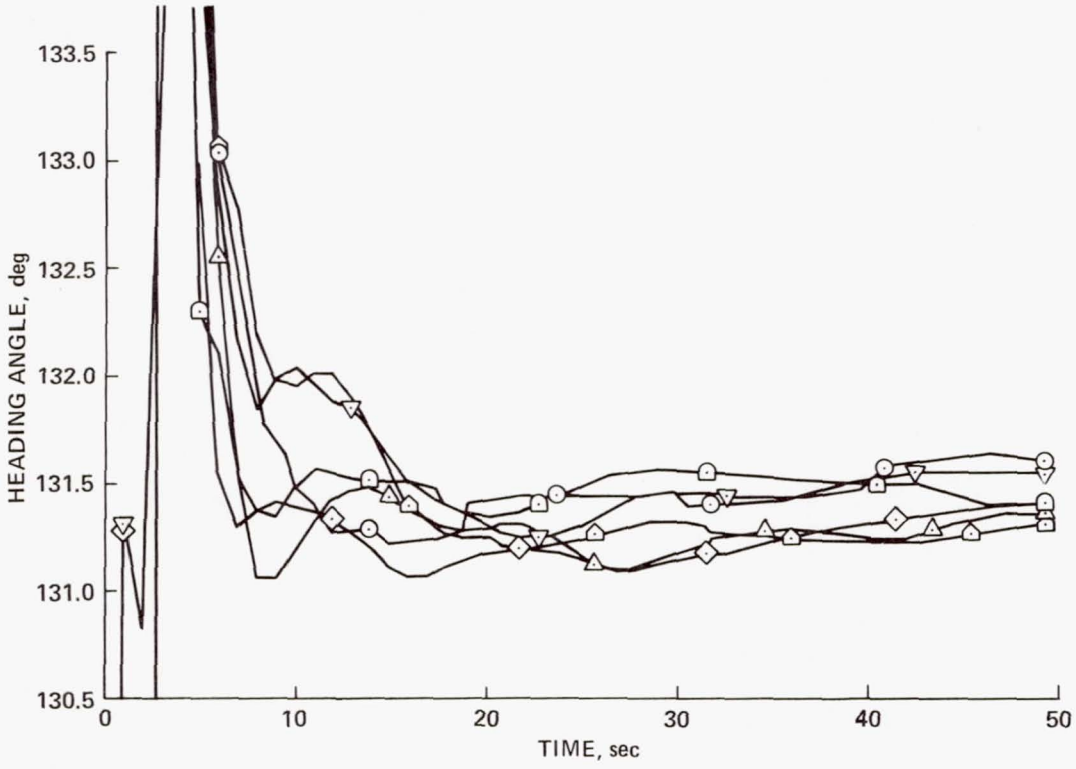

Figure 21.- Estimates of heading angles versus alignment time for six static tests.

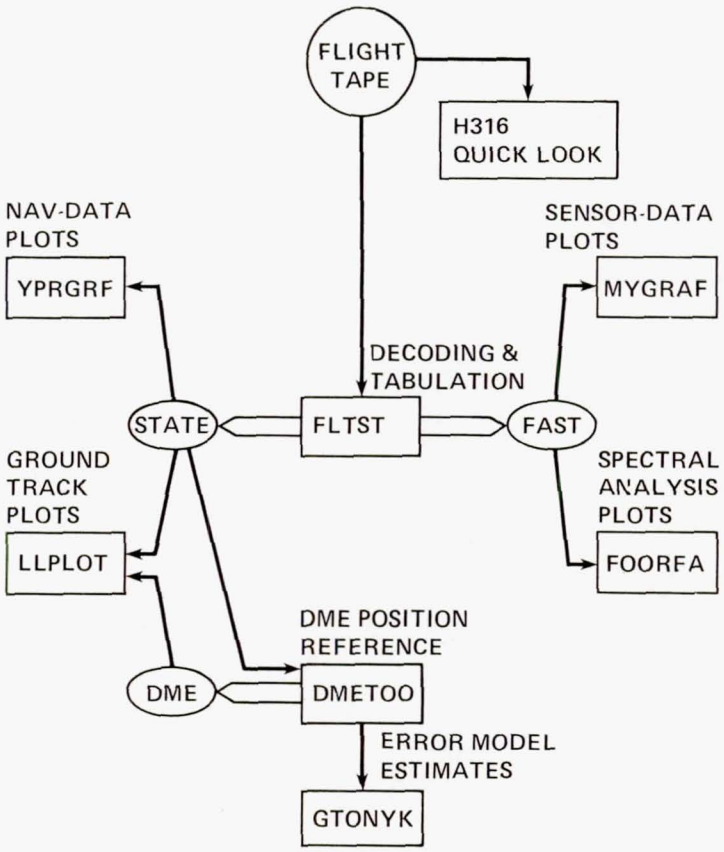

Figure 22.- Tetrad test-data-reduction elements.

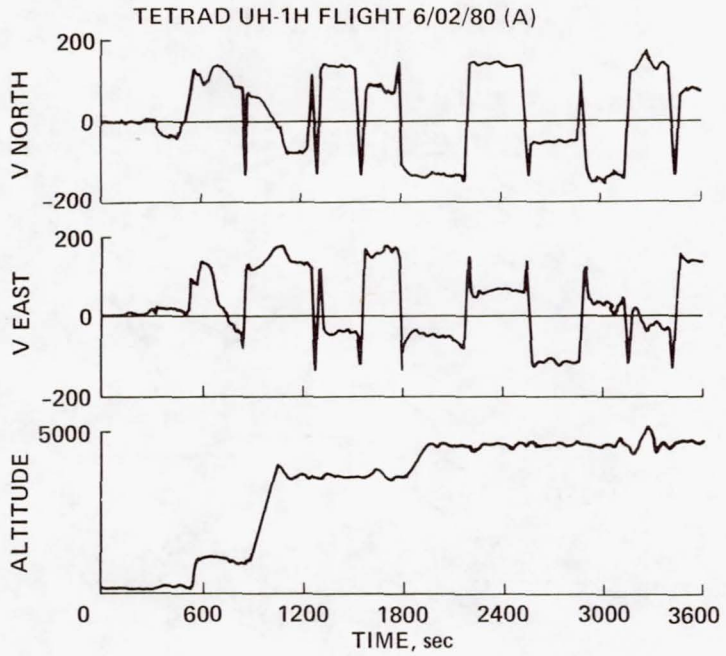

Figure 23.- Velocity and attitude output of YPRGRF program.

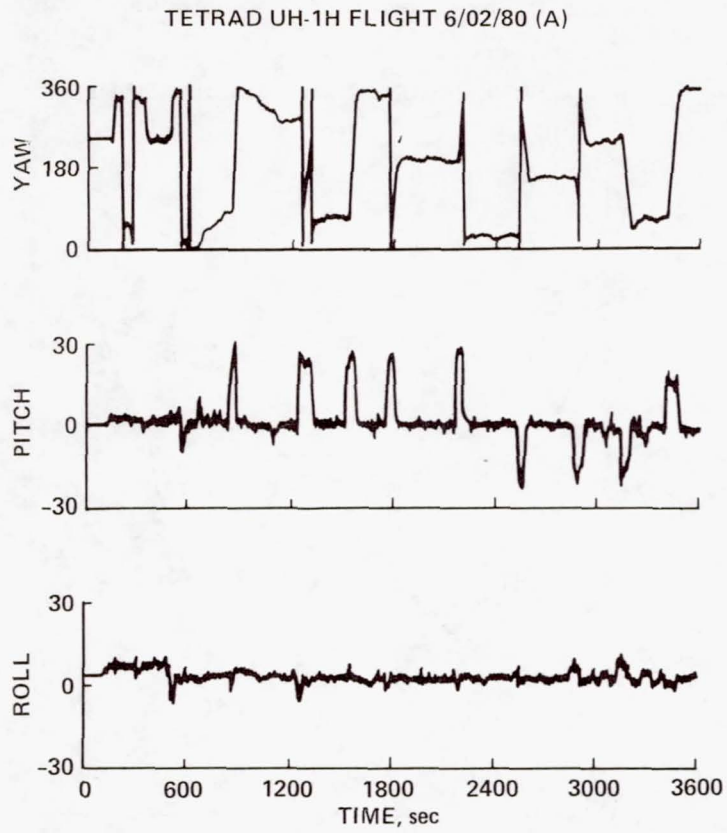

Figure 24.- Attitude output of YPRGRF program.

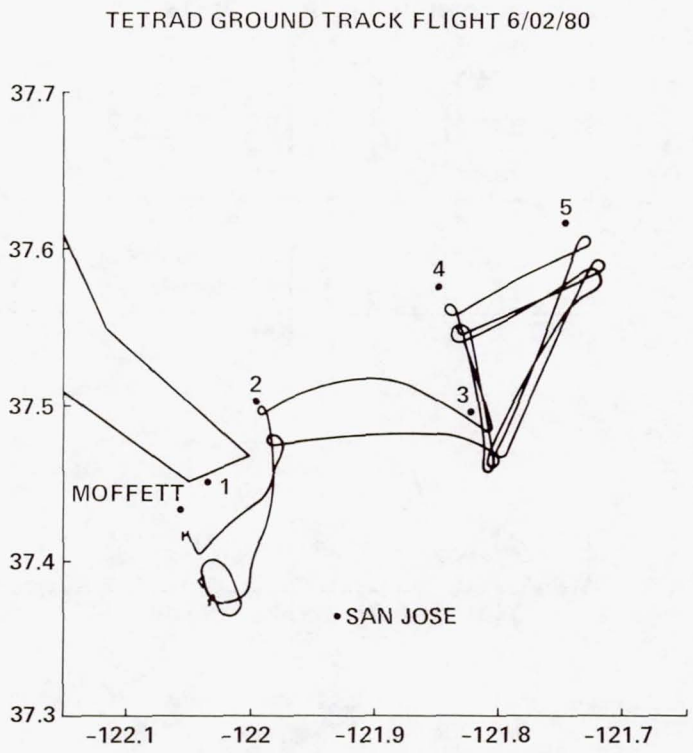

Figure 25.- LLPLOT program output of ground track from STATE.

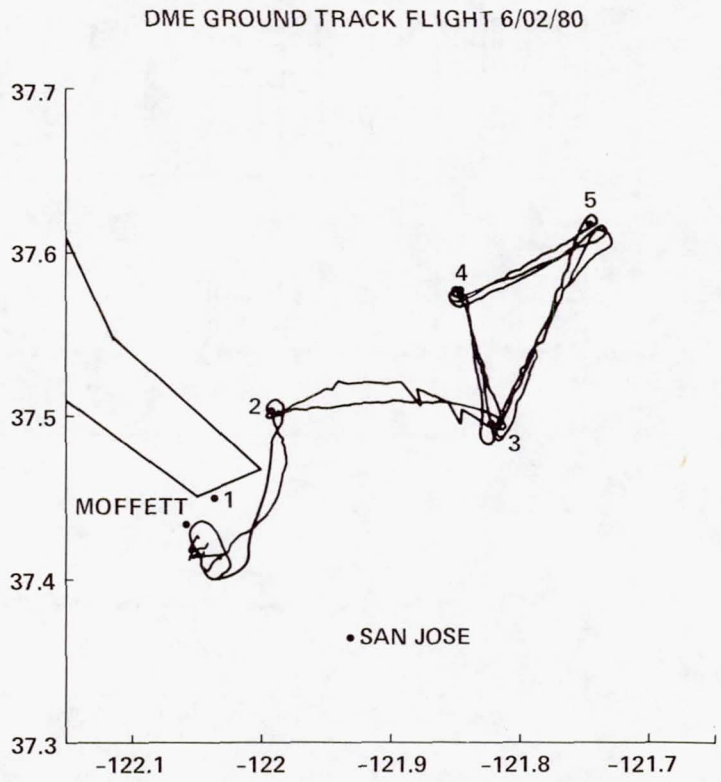

Figure 26.- LLPLOT program output of ground track from DME.

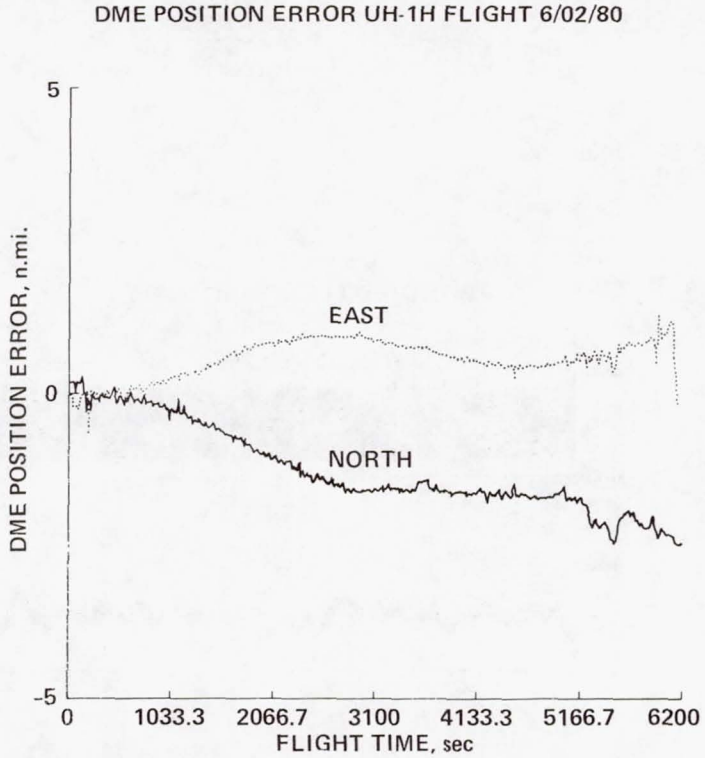

Figure 27.- DMETOO program output of position residuals from STATE.

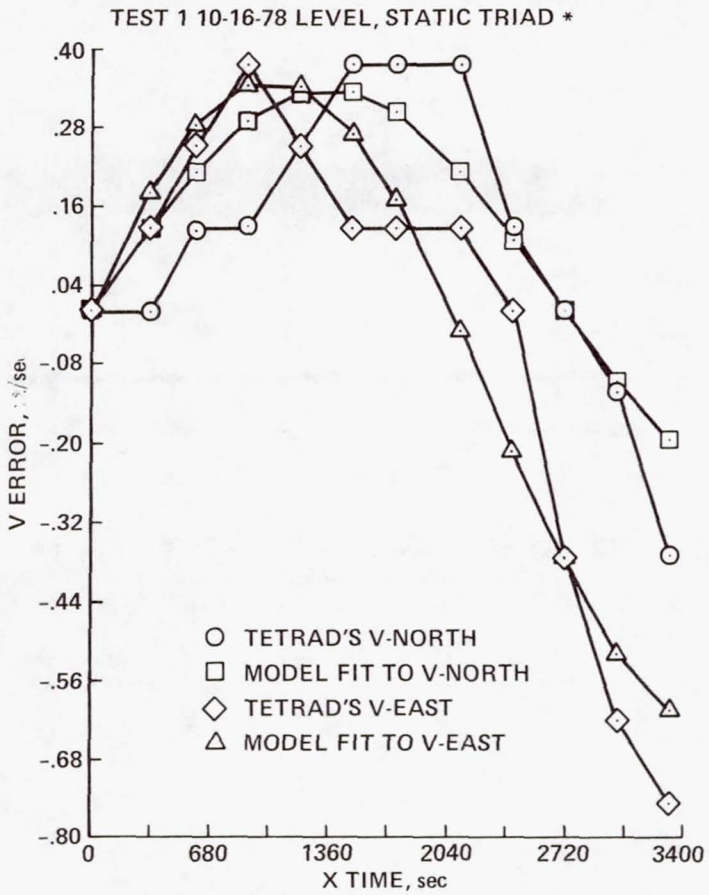

Figure 28.- STATE program output of velocity error modeling results.

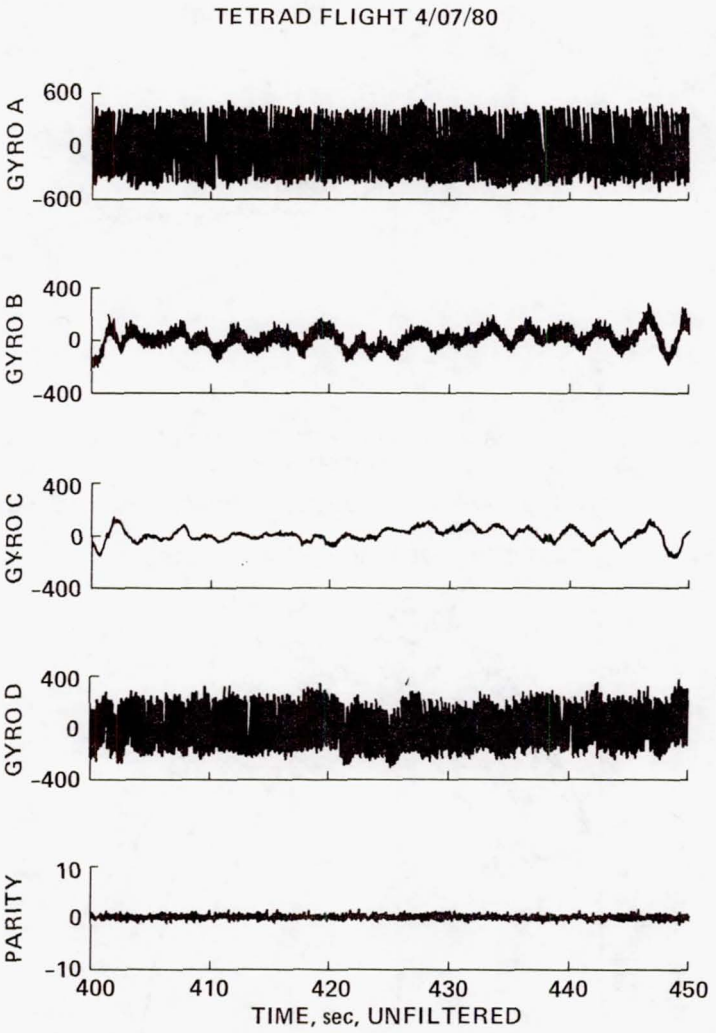

Figure 29.- Raw gyro signals and parity residual for a segment (7 April 1980) of Tetrad flight.

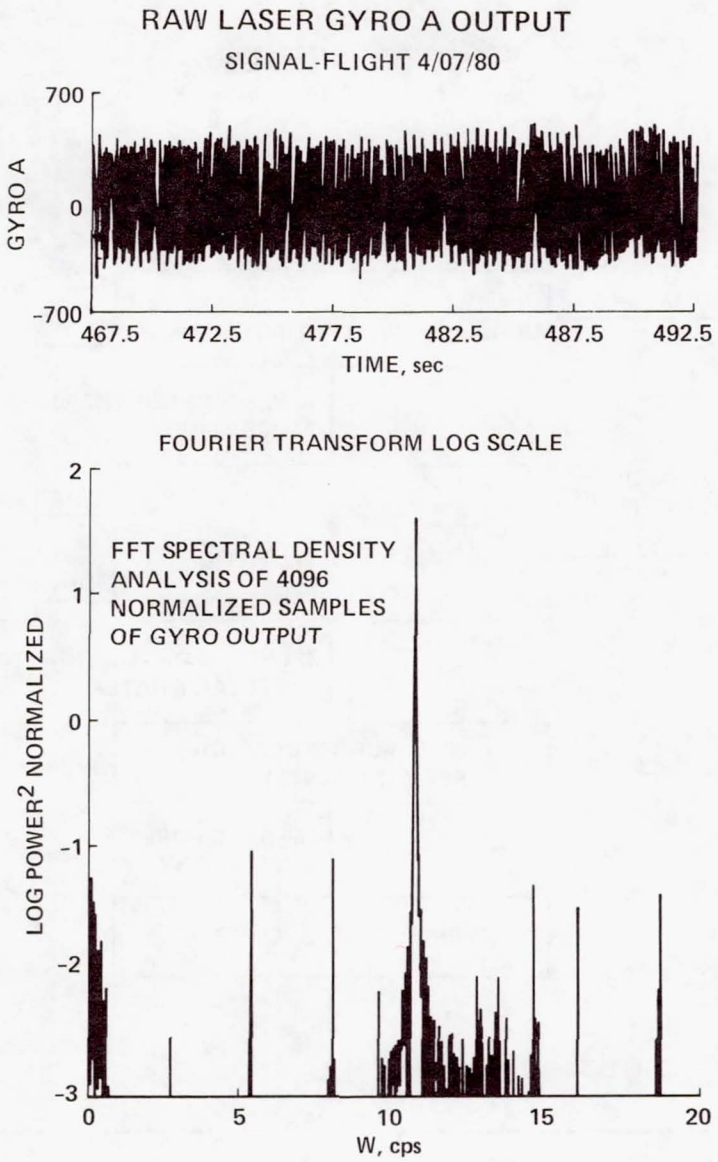

Figure 30.- Spectral density of laser-gyro A output signal.

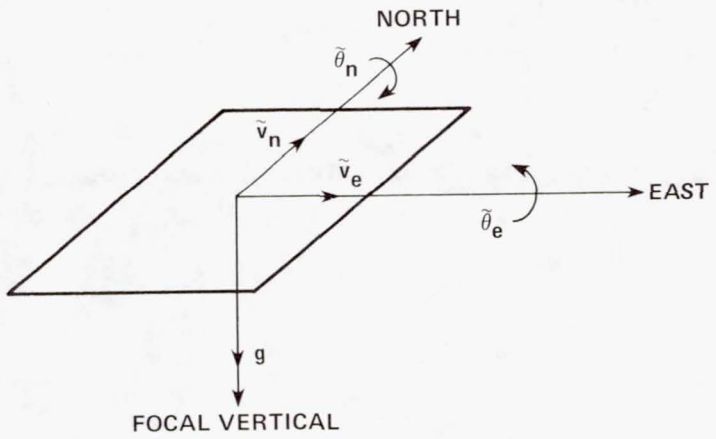

Figure 31.- Coordinate system for tilt-drift error model.

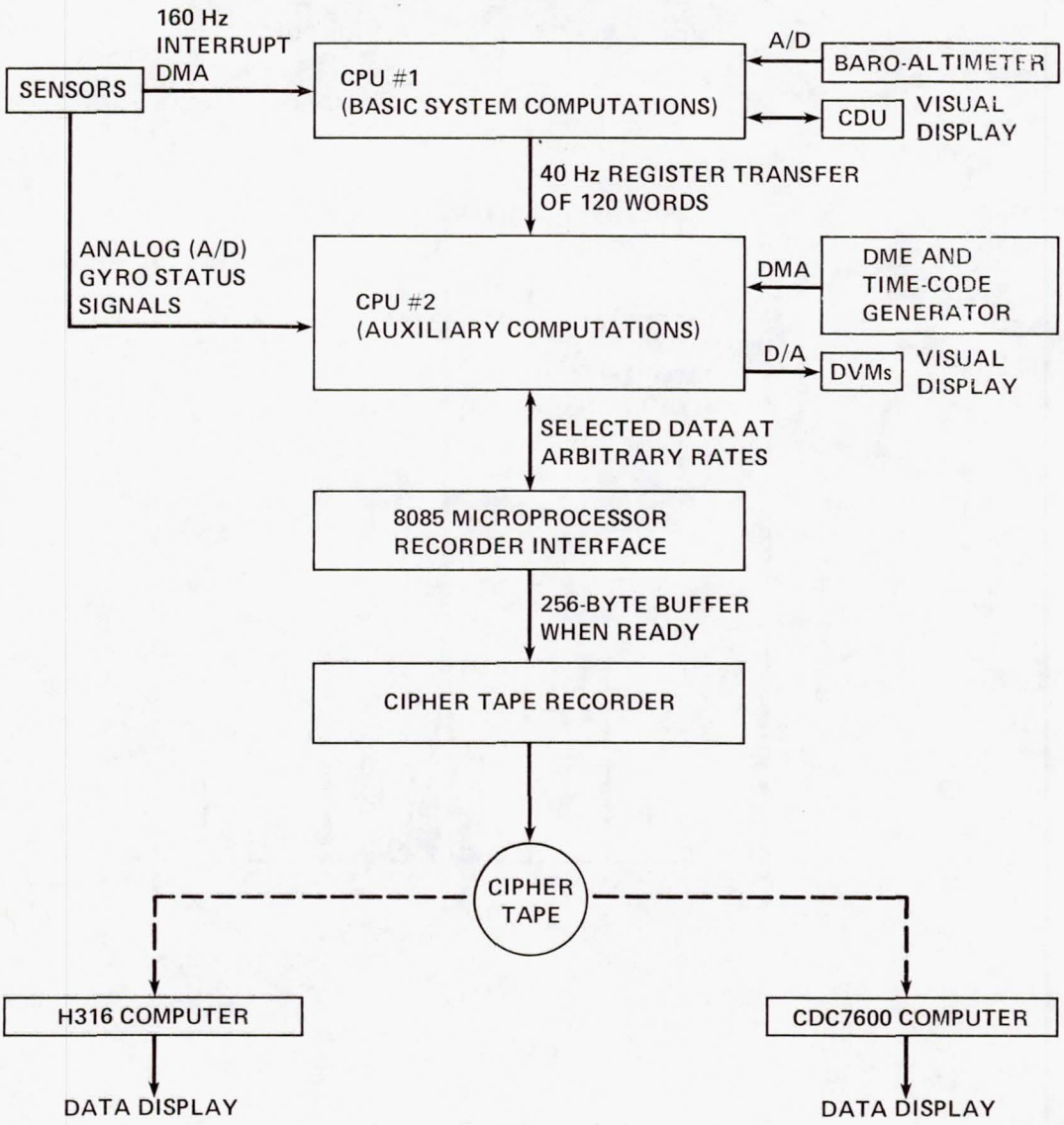

Figure 32.- Tetrad data flow.

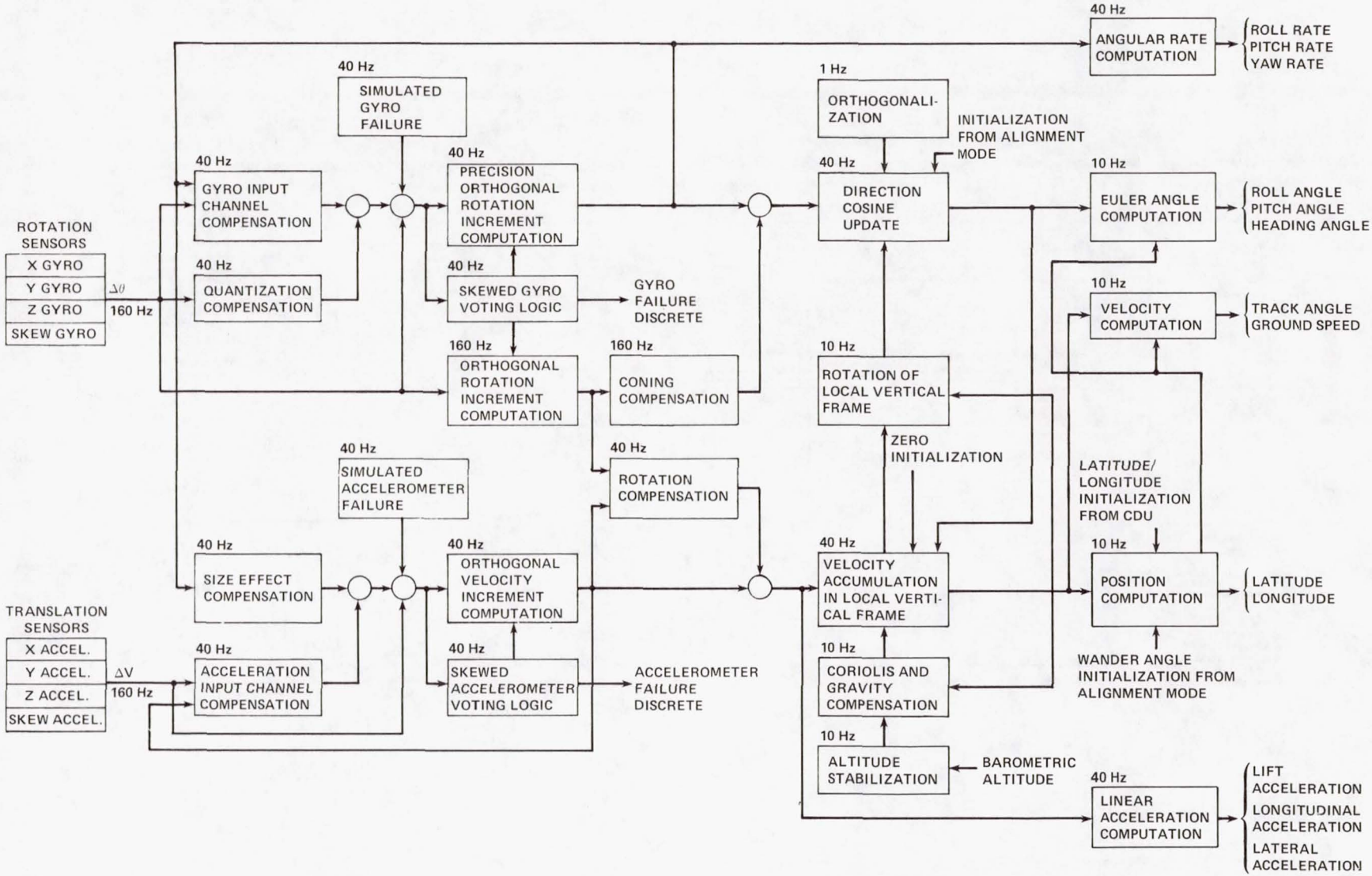

Figure 33.- Navigation-mode software.

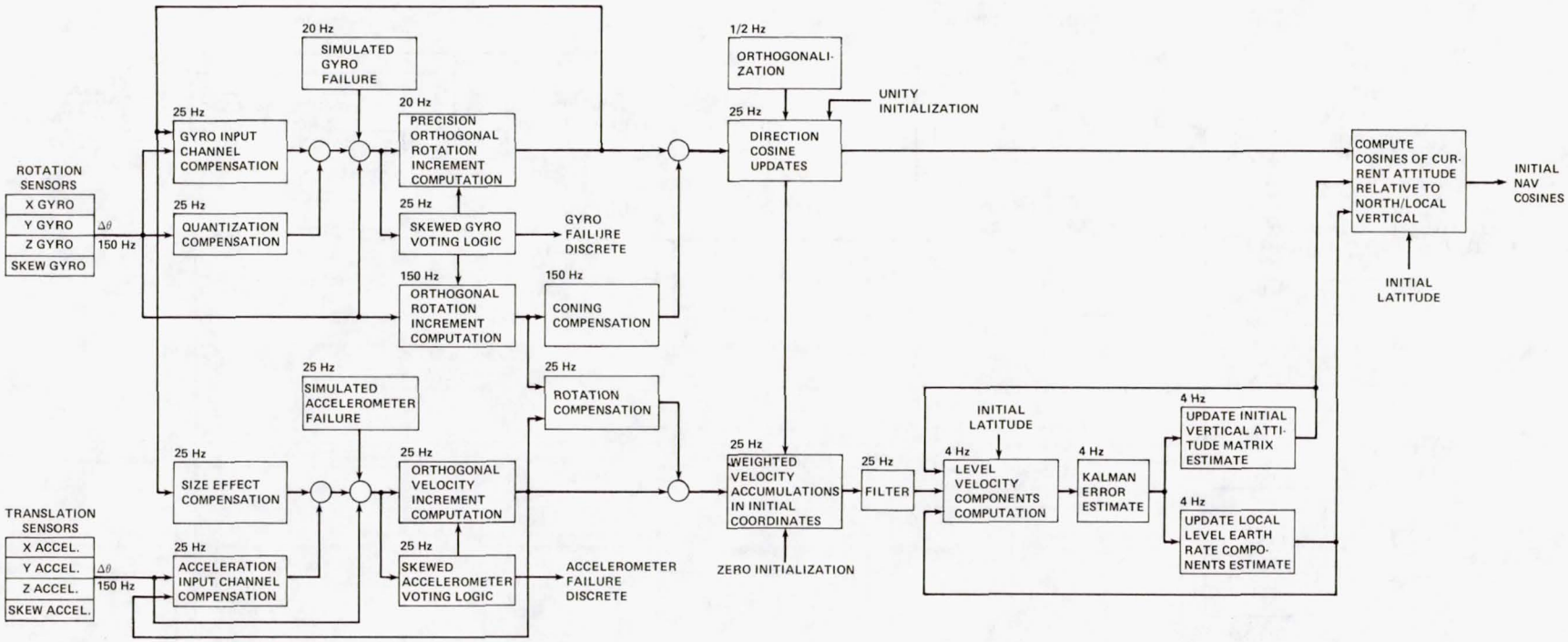

Figure 34.- Alignment-mode software.

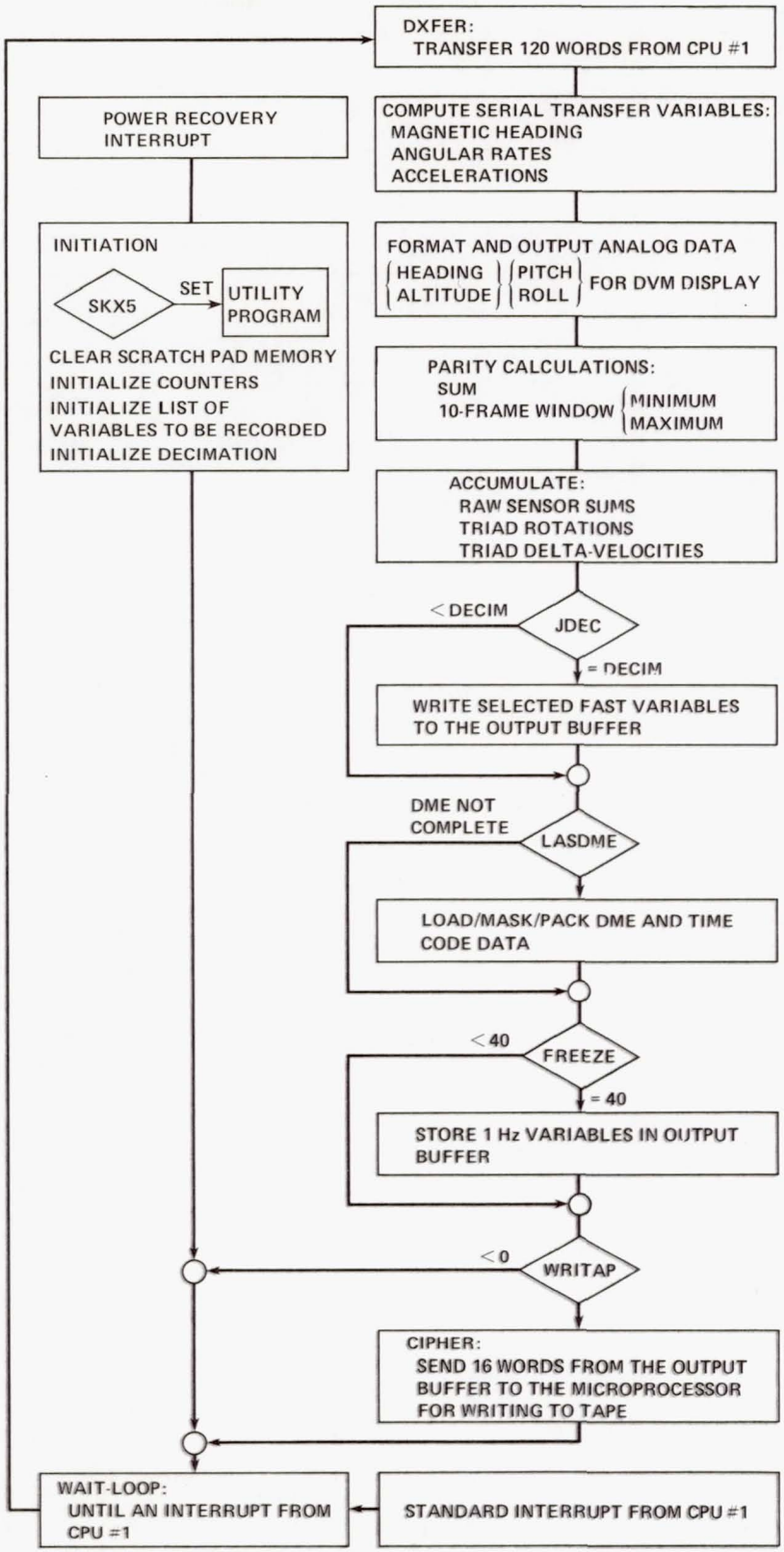

Figure 35.- CPU No. 2 software.

1. Report No.	2. Government Accession No.	3. Recipient's Catalog No.
NASA TM-84358		

4. Title and Subtitle	5. Report Date
FLIGHT TEST RESULTS OF THE STRAPDOWN RING LASER GYRO TETRAD INERTIAL NAVIGATION SYSTEM	October 1983
	6. Performing Organization Code

7. Author(s)	8. Performing Organization Report No.
R. A. Carestia (U. of So. Colorado, Pueblo, Colo.), R. J. Hruby, and W. S. Bjorkman (Analytical Mechanics Associates, Mountain View, Calif.)	A-9315
	10. Work Unit No. T-5126
9. Performing Organization Name and Address Ames Research Center Moffett Field, Calif. 94035	11. Contract or Grant No.
	13. Type of Report and Period Covered Technical Memorandum
12. Sponsoring Agency Name and Address National Aeronautics and Space Administration Washington, D.C. 20546	14. Sponsoring Agency Code 505-34-11

15. Supplementary Notes

Point of contact: Ralph Carestia, Ames Research Center, MS 210-9, Moffett Field, Calif. 94035. (415) 965-5983 or FTS 448-5983.

16. Abstract

A helicopter flight-test program undertaken to evaluate the performance of Tetrad — a strap-down, laser-gyro, inertial navigation system — is described. The results of 34 flights show a mean final navigational velocity error of 5.06 knots, with a standard deviation of 3.84 knots; a corresponding mean final position error of 2.66 n. mi., with a standard deviation of 1.48 n. mi.; and a modeled mean-position-error growth rate for the 34 tests of 1.96 knots, with a standard deviation of 1.09 knots. No laser-gyro or accelerometer failures were detected during the flight tests. Off-line parity-residual studies used simulated failures with the prerecorded flight test and laboratory test data. The airborne Tetrad system's failure-detection logic, exercised during the tests, successfully demonstrated the detection of simulated "hard" failures and the system's ability to continue successfully to navigate by removing the simulated faulted sensor from the computations. Tetrad's four-ring laser gyros provided reliable and accurate angular-rate sensing during the 4 yr of the test program, and no sensor failures were detected during the evaluation of free-inertial navigation performance. The original scale factor and cross-coupling parameter calibration made in the laboratory during initial assembly was never significantly improved upon. Repeated checks of the laser-gyro bias compensation showed it to be stable for the duration of the evaluation.

17. Key Words (Suggested by Author(s))	18. Distribution Statement
Ring laser gyro Navigation Flight test Strapdown inertial navigation	Unlimited Subject category: 04

19. Security Classif. (of this report)	20. Security Classif. (of this page)	21. No. of Pages	22. Price*
Unclassified	Unclassified	74	A04

*For sale by the National Technical Information Service, Springfield, Virginia 22161